Tryptophan-Driven Metabolomic Shift in *Acidobacteriaceae* Reveals Phytohormones and Antifungal Metabolites

Celine M. Zumkeller[1,2], Christoph Hartwig[2], Walter Lanzalonga[1], Maria A. Patras[1,2], Yang Liu[1], Michael Marner[1,2], Sanja Mihajlovic[2], Marius S. Spohn[1,2]*, Till F. Schäberle[1,2,3]*

[1] Institute for Insect Biotechnology with Focus on Natural Product Research, Justus-Liebig-University Giessen, Ohlebergsweg 12, 35392 Giessen, Germany
[2] Natural Product Department, Fraunhofer Institute for Molecular Biology and Applied Ecology (IME-BR), Ohlebergsweg 12, 35392 Giessen, Germany
[3] German Center for Infection Research (DZIF); Partner Site Giessen-Marburg-Langen, Ohlebergsweg 12, 35392 Giessen, Germany

*Corresponding author: Till F. Schäberle, till.f.schaeberle@agrar.uni-giessen.de, marius.spohn@ime.fraunhofer.de

KEYWORDS

Acidobacteriota, Phytohormones, *N6*-(*Δ2*-isopentenyl)adenine, iP, indole-3-acetic acid, IAA, PGPT, BGC

Abstract

Acidobacteriota is one of the most abundant phyla in soils and has recently attracted attention for its potential role in promoting phytosanitary benefits. The metabolomic capabilities of this phylum remain poorly characterised, with few experimentally confirmed metabolites described. To address these gaps, we combined metabolomic profiling with comparative genomic analysis to explore the functional potential of novel strains within the *Acidobacteriaceae* family. Genome mining across the phylum for plant-growth-promoting traits revealed the presence and taxon-specific enrichment of genes related to phytohormone production, as well as other genes associated with plant-beneficial microorganisms. When tryptophan was added to the cultivation medium, it triggered a strong metabolic response in the strains, resulting in measurable changes in the production levels of phytohormones such as indole-3-acetic acid and indole-3-pyruvate. Building on these findings, we examined the metabolic reprogramming caused by tryptophan supplementation, which suppressed the growth of phytopathogenic fungi, leading to the identification of malassezindoles and pityriacitrins as active agents. This was confirmed by isolating and elucidating the structure of pityriacitrin B and one of its methyl esters through NMR studies. Overall, these findings shed light on the previously unexplored metabolic potential of the Acidobacteriota phylum, emphasising its ecological importance for phytosanitary applications.

Importance

Despite their ubiquity and genomic diversity, the functional metabolism of members of the Acidobacteriota has largely remained uncharacterised. This study links genomic predictions to experimentally verified metabolomic outputs of Acidobacteriaceae, demonstrating tryptophan-responsive metabolic shifts translating to phytohormones and metabolites suppressing fungal growth.

Our work underscores the emerging role of Acidobacteriota as important contributors to soil ecosystem functioning and plant–microbe interactions.

Introduction

Ubiquitous across various ecosystems, including soil (1–3), marine sediments (4), wetlands (5–7), as well as extreme environments such as permafrost (8) and acidic mine drainages (9), Acidobacteriota represent one of the most widespread bacterial groups (10). The phylum is phylogenetically diverse (11), classified into 26 subdivisions (12) based on 16S rDNA sequencing. Despite their ubiquity, the Acidobacteriota have historically been underexplored due to the limited availability of cultured representatives, which has restricted experimental characterisation and genomic insights (13). Today, the availability of high-quality metagenome-assembled genomes, combined with the growing number of cultured representatives and isolate genomes, has significantly broadened our understanding of the metabolic capabilities and ecological roles of this phylum (13–15).

Initially described as slow-growing oligotrophs (16) With limited metabolic dynamics, adapted to nutrient-depleted environments, modern insights now reveal their versatility and critical involvement in biogeochemical processes, including sulphur (17) and nitrogen (18) cycling as well as H_2 consumption (19). Furthermore, they can degrade plant-derived polysaccharides using their rich repertoire of carbohydrate-active enzymes, such as cellulases, chitinases, and xylanases (20). Finally, early studies dating back to 2006 proposed a substantial potential for secondary metabolite production by biosynthetic gene clusters, identifying novel Polyketide synthase gene clusters of acidobacterial origin from soil (21, 22). Subsequent genomic (23) and metagenomic studies confirmed this finding, identifying biosynthetic-gene-cluster (BGC)-enriched lineages such as the *Acanthopleuribacteraceae* (24) and the genus *Candidatus Angelobacter* (22). Yet, translating bioinformatic findings into experimental validation remains difficult and still requires the availability of culturable representatives. Notably, Leopold-Messer *et al.* (24)successfully retrieved marine sponge symbiont strains from the *Acanthopleuribacteraceae* family, marking the first description of non-ribosomal peptide (NRP)-polyketide (PK)-derived secondary metabolites from this phylum (24).

To overcome these gaps, various cultivation approaches have been developed to selectively favour acidobacterial growth and retrieve single-isolate strains from complex environmental samples (3, 25–27). These approaches have significantly increased the number of isolated strains; however, they still only represent a fraction of the predicted phylum diversity. Most of the strain isolates are retrieved from soil (23), where Acidobacteriota have consistently shown high abundances, ranging from 20% to 40% of the detected 16S rRNA(28, 29) sequences. Cultivation strategies often utilise plant polymers for Acidobacteriota enrichment (25, 26, 30), providing insight into their predicted function in enhancing soil health by degrading undigestible plant polymers and improving nutrient content in the soil. Consequently, several studies investigate the potential plant-growth-promoting (PGP) effects of the phylum. In 2016, the first evidence of a direct plant-interaction was described by Kielak *et al*. (31). They found that some acidobacterial strains produced IAA and also demonstrated a PGP effect on the model plant *Arabidopsis thaliana* (31). Moreover, Acidobacteriota are recognised for synthesising hopanoids (32), bacterial analogues of sterols, known to enhance stress tolerance in soil bacteria as an integral component of the bacterial membrane. Their unique exopolysaccharide production (33, 34) further suggests a potential ability to endure dry conditions and possible roles in sustaining plant health, e.g., protecting against desiccation. Complementary metagenomic and meta-transcriptomic studies have revealed a significant enrichment of genes related to PGP. Gonçalves *et al.* (2024) profiled 758 soil-associated metagenome-assembled genomes (MAGs) and identified plant-growth-promoting-traits (PGPTs) involved in phytohormone production, nitrogen fixation, phosphorus

solubilisation, siderophore production, and exopolysaccharide biosynthesis (20). These traits were explicitly enriched in certain families of the Acidobacteriota, namely *Acidobacteriaceae*, *Pyrinomonadaceae*, and *Koribacteriaceae*. Meta-transcriptomic evidence shows that these traits are actively transcribed in their respective environmental context (20). Furthermore, transcriptomic research has demonstrated the metabolic dynamics and responsiveness to external stimuli of cultured Acidobacteriota strains. For instance, *Acidobacterium capsulatum* responds to oxygen deprivation by switching to a respiro-fermentative state, resulting in the production of acetate and ethanol —a strategy that allows for survival in habitats with fluctuating O_2 levels, such as soil (35). The oligotrophic lifestyle typical of the Acidobacteriota has been investigated in a *Granulicella* species, which responds to high-carbon availability by upregulating stress-related genes, indicating sensitivity to nutritional changes (36). While many ecological functions are inferred from meta(transcriptomics) data, experimentally generated metabolomic data remain limited, primarily focusing on the characterisation of membrane lipids and their production in response to different cultivation parameters such as temperature, pH, and O2 (37, 38).

To address these gaps, we integrated metabolomic profiling with comparative genomic analysis to investigate the functional potential of novel strains of the *Acidobacteriaceae* family. Phylum-wide genome mining for PGPTs revealed the presence and taxon-specific enrichment of genes associated with phytohormone production, as well as additional genes related to PGP effects. The addition of tryptophan (Trp) to the cultivation medium elicited a strong metabolic response in the strains, resulting in quantitatively determined shifts in the production levels of the phytohormones indole-3-acetic acid (IAA) and indole-3-pyruvate (iP). Prompted by these findings, we evaluated the metabolic reprogramming induced by Trp supplementation, revealing suppressive effects on the growth of phytopathogenic fungi, and subsequently identified pityriacitrins and malassezindoles as the causative agents. Collectively, these findings highlight the previously underexplored metabolic space of the Acidobacteriota phylum, underscoring its ecological significance for phytosanitary purposes.

Results and Discussion

Result 1 - Diverse Cultivation Strategies Reveal the Production of Phytohormones

Extensive metagenomic data from globally distributed bioresources indicate an underexplored biosynthetic and ecological potential of the Acidobacteriota phylum. During our ongoing efforts to isolate and bioprospect bacterial diversity for its potential in the production of natural products and related environmental functions, we retrieved three Acidobacteriota strains from termite nest material (25) and one strain from a German soil sample (39). To evaluate their biosynthetic potential, we isolated their total DNA together with that of the type strain *A. borealis* DSM 23886 and performed whole-genome sequencing. The generated genomic data underwent quality check using CheckM2 (40). By applying recognised quality criteria (completion >90% and contamination <5% (41)), one assembly (FHG110206) was disqualified for further analysis, while the other three assemblies were used for genome-based taxonomic affiliation by the genome taxonomy database (GTDB) (42) (Supplementary Table 1). This positioned the termite nest-associated strains as members of the genera *Acidobacterium* (FHG110202) and *Terracidiphilus* (FHG110214), while the soil-associated strain FHG110511 was identified to be an *Edaphobacter*. All three strains belong to the family of *Acidobacteriaceae* (collectively referred to as FHG *Acidobacteriaceae* in this manuscript). Thus, we selected further available strains of this family (*Edaphobacter aggregans* DSM 19364*, Acidobacterium sp.* S8*, Silvibacterium bohemicum* S15*, Acidicapsa borealis* DSM 23886*, Granulicella rosea* DSM 18704, and *Bryocella elongata* DSM 22489)(Table S1) and performed an extensive OSMAC (one-strain-many-compounds) approach (43), conceptualised to increase the likelihood of covering a favourable condition for the strains to proliferate and promote gene expression. To this end, we modified the

carbon sources, vessel size, and shaking speed, and applied solidification and surface texture methods using quartz or ceramic beads, potentially enabling the surface attachment of the cells. Cultivations were performed on a 100 ml scale using 300 ml Erlenmeyer flasks or at a 4 ml scale using 24 well Duetz system plates (Table S2). Samples were taken on days 5, 7, 10, 12, and 14 of the respective cultivations. The generated samples were dried by lyophilisation and extracted with methanol, resulting in a total of 892 organic extracts. An aliquot of each extract was reconstituted in dimethyl sulfoxide (DMSO) and used to determine the antimicrobial bioactivity by screening against the bacterial indicator strains *Escherichia coli* ATCC 35218, *Bacillus subtilis* DSM 10, and *Mycobacterium smegmatis* ATCC 607, as well as the fungus *Candida albicans* FH2173. This, however, did not reveal any reproducible antimicrobial effect enabling traceability of a causative agent (data not shown). Furthermore, we conducted a bioactivity-independent and metabolomics-driven bioprospecting campaign. Initially, we focused on the metabolic profiling of strains FHG110202 and FHG110206 and assessed the metabolic composition of their generated extracts (n = 244, including media controls) analytically by performing ultra-high-performance liquid chromatography coupled to high-resolution mass spectrometry (UHPLC-QTOF-HR-MS). Molecular features (*m/z*, retention time) were detected and aligned into buckets. Combining timepoints for each strain-media combination and presence-absence analysis led to 72 conditions (including media controls) with 20285 features present and distributed into 2747 buckets (Figure S1).To assess the effect of the medium on the metabolome of the strains, we filtered medium-derived features (n=1795). Pairwise Jaccard distances between samples were ordinated by principal coordinates analysis (PCoA) for strains FHG110206 and FHG110202 (Figure 1A). Metabolomic profiles clustered mainly by medium (colour code) and vessel size (top, left cluster) rather than by strain. We also observe a distinct cluster for medium containing quartz beads (bottom, right cluster). A PERMANOVA analysis confirmed this observation, suggesting a strong OSMAC response. The medium identity accounts for 87% of the variance among strain extracts (F=7.09, p=0.001), while the strain identity within the same medium explains a much smaller share (1.7%, F=0.77, p=0.001). Within the small-scale set, the bead condition explained 29.2% of the differences (F = 7.64, p = 0.001), consistent with the observed quartz-bead cluster. Thus, metabolomes are primarily influenced by the medium and vessel size, with only a small strain-level difference. We also plotted unique features of strain-produced metabolites for individual media conditions (Figure 1B), and found that in both strains (FHG110202:FHG110206), media F (87:125), U (65:64), W (86:86), and X (197:116) are enriched in unique features compared to the average unique feature number across all media (22.2:20.7). This indicates that the large-scale cultivation size in 300 ml Erlenmeyer flasks yields a more distinct metabolome compare to the small-scale cultivation in 24-well plates.

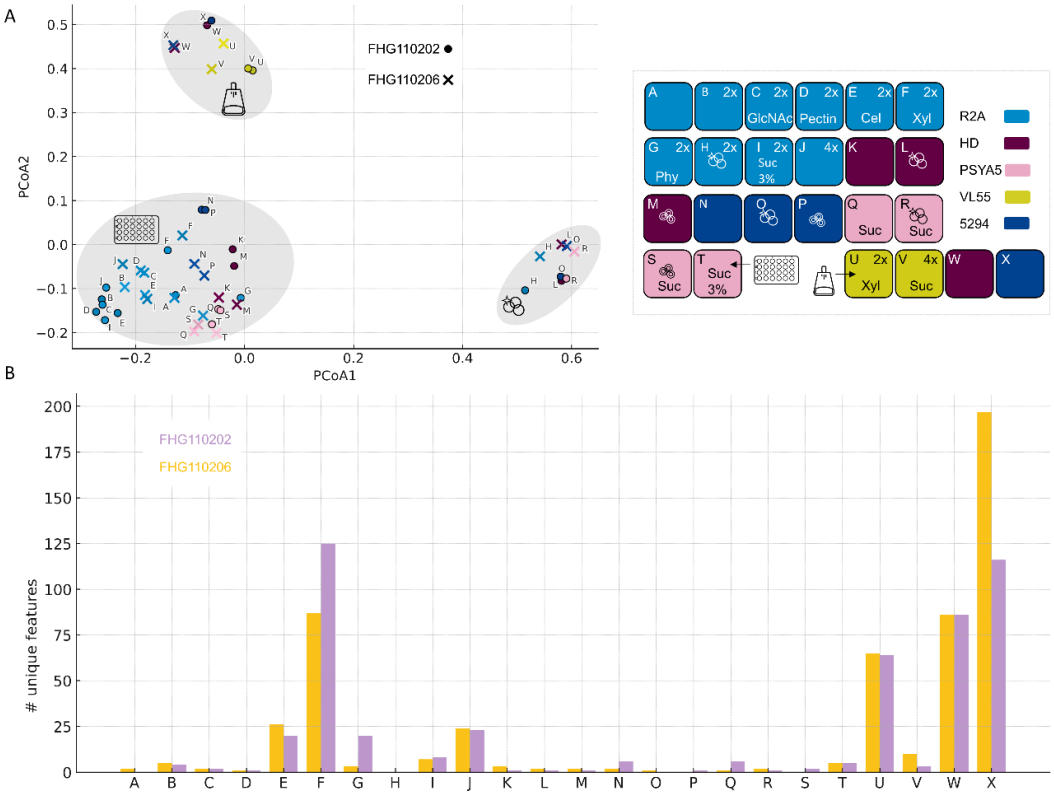

Figure 1 OSMAC metabolome variation by medium, strain, and cultivation scale. The legend details the media compositions (A-X), based on base-media colour, concentration, additives, and bead status. Samples labelled A-T were cultivated in 24-well plates (small-scale), while U-X were grown in 300 ml Erlenmeyer flasks. If not stated otherwise, additives were supplied in concentrations of GlcNAc, N-acetyl-glucosamine (0.05%); Cel, cellobiose (0.5%); Xyl, xylan (0.5%); Phy, phytagel (0.8%); Suc, sucrose (0.5%). **(A) PCoA of control-filtered LC/MS presence/absence fingerprints using Jaccard distance**. Samples are labelled by the medium letter (A-X) and coloured by base-medium (see legend). Samples from FHG110202 are marked with circles, and FHG110206 with crosses. Light grey ellipses highlight visually distinct clusters, and icons indicate their common features: large-scale flask cultivation (flask), small-scale 24-well cultivation (24-well plate), and quartz beads containing samples (circles). **(B) Number of unique features per medium (A-X) and strain as clustered bars**. Strains are indicated by colour: FHG110202 (light purple), FHG110206 (yellow). Unique features are defined as not being present in any medium control and only present in the respective medium, but not in any other medium.

The detected metabolite features were matched against our in-house reference compound MS database, which contained approximately 1300 structurally characterised microbial metabolites at the time of data processing. By comparison of mass to charge ratios and retention time, we were able to annotate the phytohormone IAA in the extracts of our FHG *Acidobacteriaceae* strains with a confidence level 1 (Identified metabolite: as proposed by the Chemical Analysis Working Group of the Metabolomics Standards Initiative (44)). The production of the phytohormone IAA has been reported for members of the *Acidobacteriaceae* (31). To systematically describe the cultivation conditions that favour IAA production, we visualised the peak area of IAA in FHG110202 as an example across all tested media and setups (Figure S2). While IAA was not produced under conditions leading to the isolation of the strains (VL-55 base media), it became detectable in more complex media. Among these, R2A-based cultivation, with agitation, consistently showed the best IAA production. To further analyse the phytohormone production of FHG110202, we included additional standards: Kinetin (CAS 525-79-1), Trans-zeatin (CAS 1637-39-4), Indole-3 Butyric Acid (CAS 133-32-4), Brassinolide (CAS 72962-43-7), jasmonic acid methyl ester (CAS 39924-52-2), jasmonic acid (CAS 77026-92-7), abscisic acid (CAS 21293-29-8), indole-3-propionic acid (CAS 830-96-6), 1,2-Diphenylurea (CAS 102-07-8) and *N6*-(*Δ2*-Isopentenyl)adenine (iP)(CAS 2365-40-4) to our *in-house* reference database and explicitly checked for their presence in the generated crude extracts. This revealed the presence of the cytokinin

193 iP at a confidence level of 1. The detection of cytokinin iP as a biosynthetic product of members of the
194 Acidobacteriota phylum is a new finding.

195 Result 2 – Biosynthetic Potential of the Acidobacteriota phylum

196 To complement the metabolomic workflow, we evaluated the genomic potential of our
197 FHG *Acidobacteriaceae* and comparatively aligned it to the broader Acidobacteriota landscape.
198 Therefore, we initially searched for publicly available genomes matching the criteria Query:
199 "Acidobacteriota" NOT "anomalous" in the NCBI database. This yielded 1428 genomes that underwent
200 quality control using CheckM2 (40) (Figure S3), applying the above-defined quality criteria. This
201 resulted in a final dataset comprising 618 genome assemblies. Overall, most of the analysed genomes
202 were retrieved from metagenomes (n = 533; 86%) (Supplemental Table 1). A detailed bioinformatic
203 analysis of this dataset is reported in the Extended Methods and Results section of the supplementary
204 information. The taxonomic affiliation was established by GTDB (42) and the generated multiple-
205 sequence alignment was used to build a phylogenetic tree. The bioinformatically predicted features
206 of each strain were assigned and visualised within the tree using iTOL (45). The genomes in the dataset
207 span 12 classes (Figure 2), dominated by the *Acidobacteriae* (n = 242), *Blastocatellia* (n = 130) and
208 *Vicinamibacteria* (n = 98), which also represent the majority of today's strains brought to culture
209 (76/86-88%). To evaluate the biosynthetic potential of the Acidobacteriota phylum, we predicted
210 BGCs using the standalone version of antiSMASH (46). In total, 3865 BGCs were detected in the
211 genome dataset. The most abundant BGC class in the dataset is ribosomally produced and post-
212 translationally modified peptides (RiPPs) (n = 1152, 30%), followed by non-ribosomal peptide
213 synthetases (NRPSs) (n = 978, 26%) and terpenes (n = 777, 13%). The total average cluster number per
214 class in our acidobacterial dataset is 6.2 ± 4.4 BGCs. The *Acidobacteriae* class exhibits the highest
215 overall number of BGCs, with an average of 7.4 ± 3.7 BGCs per genome, followed by UBA6911 and
216 Mor1, with 6.3 ± 2.5 and 5.8 ± 2.1 BGCs, respectively. Dedicated analysis of the FHG *Acidobacteriaceae*
217 revealed an average of 9 ± 3.46 BGCs, slightly higher than for the overall phylum and the
218 *Acidobacteriae* class value, but comparable to the overall family value (7.9 ± 3.0). Again, the most
219 represented group of BGCs is the RIPPs (sum: 10), followed by the terpenes (sum: 7) and the NRPS
220 (sum: 4) BGCs. Notably, the *Holophagae* class, despite having an average BGC number of 5.1, exhibits
221 a high standard deviation of 10.5, indicating a high potential for some of its representatives. This value
222 can be accounted for by the *Acanthopleuribacteraceae* (Z-score: 3.5), showing high BGC counts of >40,
223 seven times higher than the average Acidobacteriota genome. Intriguingly, the first acidobacterial NPs
224 recently isolated also come from this family (24). While these talented strains have been isolated from
225 marine animals, Acidobacteriota are known to be habitat generalists with a wide distribution,
226 primarily found in soil ecosystems. They are characterised by a variety of extracellular products, such
227 as biosynthetic gene clusters (BGCs), which are more extensive in soil-preferring lineages compared
228 to their non-soil-preferring relatives, including the *Holophagae*. Although analysing biosynthetic
229 potential at the class level is useful, our analysis demonstrates the advantages of examining family
230 and genus levels. This approach helps identify the most promising taxonomic hotspots for discovering
231 new natural products (NP).

232 To complement the evaluation of the Acidobacteriota phylum, we performed sequence similarity
233 calculations on the total of 3865 BGCs in our dataset using BiG-SCAPE (47), including the MiBIG
234 reference BGCs, and applied a cutoff of 0.5. 1651 BGCs remained as singletons, contrasted by the
235 largest Gene Cluster Family (GCF) that consists of 25 members, all from the *Acidobacteriae* class.
236 Twenty-five GCFs are specific to one respective taxonomic class (Figure 1B, Figure S8); most of these
237 GCFs contain more than 10 representatives (16/25), indicating clear taxonomic conservation. This
238 taxonomic conservation is further illustrated by comparing the GCF composition of the different

strains using cosine distance and visualising this similarity as uniform manifold approximation and projection (UMAP) (Figure S9). Here, strains belonging to the same taxonomic classes cluster within the visualisation, indicating overall conservation between phylogenetic groups. However, sequence similarity calculations revealed that the FHG *Acidobacteriaceae* do not share any of their clusters (Figure S8). Further, alignments with MiBIG Reference BGCs and confirmation by CORASON alignment (47) revealed a co-clustering of 7 acidobacterial BGCs in four GCFs (Figure 2), showing compositional BGC similarity to, e.g. the myxochromide and the occidiofungin A-reference BGCs (SI-extended methods and results). Intriguingly, the latter is a match to our strain FHG110511, harbouring a PKS/NRPS hybrid BGC that clusters in GCF1959 with the occidiofungin A reference BGC (MiBIG BGC0001711) at a pairwise identity of 70.4% (Figure S11). Occidiofungin A is a *Burkholderia contaminans*-produced NP that exhibits broad antifungal activity and is in early clinical development (gel OCF001, phase 1) for use against multidrug-resistant vaginal yeast (*Candida* spp.) infections (48, 49). The comparative evaluation of the NRPS and NRPS/PKS hybrid core gene architecture revealed a highly conserved module arrangement with certain discrepancies in predicted A-domain specificity. Testing of the strain's organic extracts against *C. albicans,* however, showed no antifungal activity.

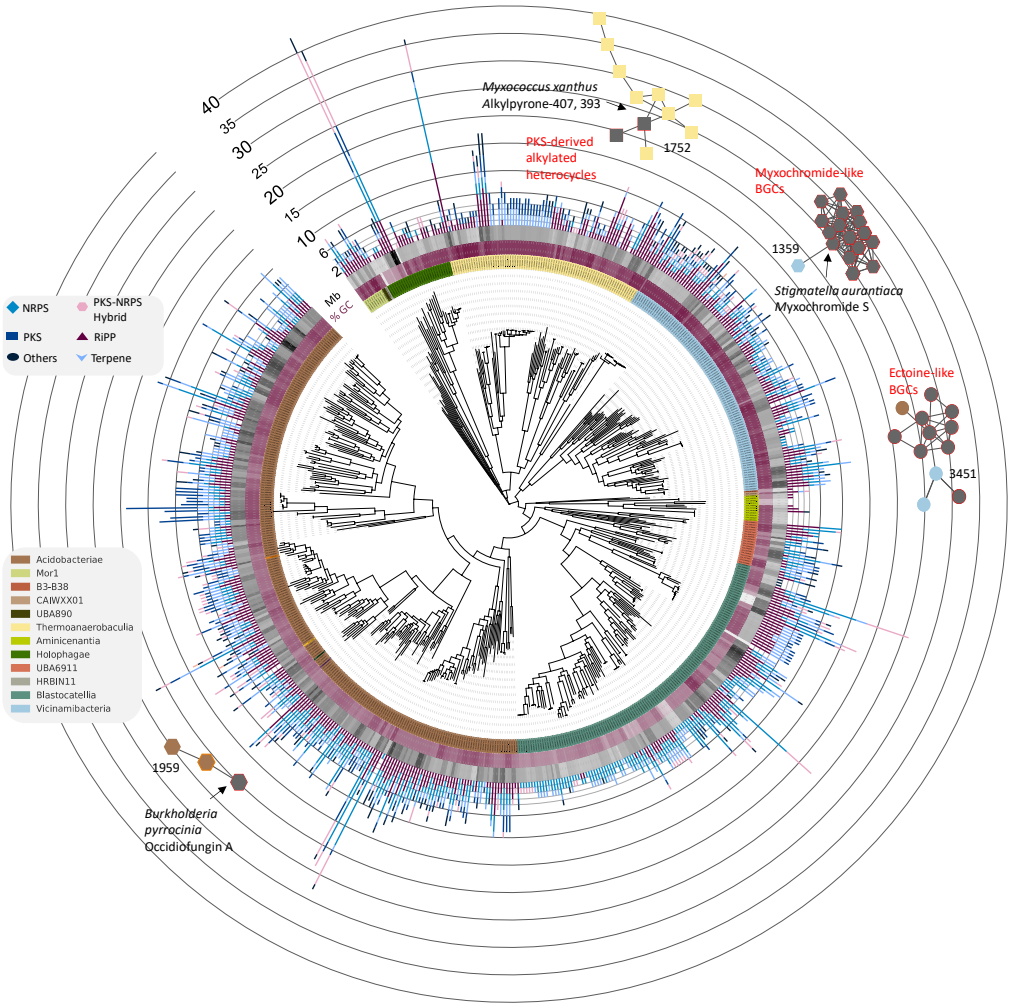

Figure 2: BGC composition of the Acidobacteriota Phylum and BiG-SCAPE Network of acidobacterial BGCs clustering with MiBIG reference clusters. Multiple Sequence Alignments generated by GTDB were used to create a phylogenetic tree of 618 representatives of the Acidobacteriota. Twelve acidobacterial classes were identified by GTDB and are indicated by different colours (ring 1). FHG strains are colour-coded as follows: FHG110214 (green), *A. borealis* DSM 23886(purple), FhG110202 (yellow), and FhG110511 (orange). Ring two indicates the genome size of the individual representatives, ranging from black (larger genomes) to grey (smaller genomes). Bar charts indicate the total number of antiSMASH-detected BGCs, differentiated into different BGC types.

254 The occidiofungin-like BGC represents a singleton hit in respect to multimodular NRPS, PKS or hybrid
255 systems within the genomes of the FHG *Acidobacteriaceae*, indicating a generally underdeveloped
256 talent of our strains to produce structurally complex NPs and a possible reason for the lack of
257 antimicrobial activity observations during our initial bioprospecting campaign.

258 Result 3 – Tryptophan Supplementation Increases IAA but Decreases iP Production in 259 Acidobacteriaceae without Enhancing Barley Seedling Biomass

260 During the metabolomic-based inspection of the OSMAC experiment, we identified the biosynthetic
261 potential of our FHG *Acidobacteriaceae* to produce the phytohormones IAA and iP. To further profile
262 the IAA and iP production of our FHG *Acidobacteriaceae* and the reference strain
263 *A. borealis* DSM 23886, we cultivated those strains in media with and without supplementation of
264 tryptophan (Trp), commonly known to increase IAA production in microorganisms (50). We performed
265 a kinetics study to analyse the influence of 0.2% Trp on the relative IAA and iP production over 14 days
266 following the methanolic extraction of the cultures. Overall, the amounts of IAA and iP increased over
267 time, reaching their highest levels on days 10 and 12 of growth (Figure 3 and S12). Indeed, the
268 supplementation of Trp enhanced IAA production significantly in all strains. In contrast,
269 supplementation of Trp consistently suppressed iP production in the analysed strains except for
270 FhG110202 and *A. borealis* DSM 23886, where this effect is less pronounced (Figure 3A). This initial
271 profiling revealed that strain FHG110214 was the most productive iP producer, while exhibiting
272 comparable productivity in IAA to *A. borealis* DSM 23886, FHG110202, and FHG110206. Based on this
273 production profile, we selected FHG110214 and *A. borealis* DSM 23886 to perform an absolute
274 quantification of phytohormones. When supplemented with Trp, *A. borealis* DSM 23886 produced IAA
275 to a final concentration of 0.326 ± 0.063 µg/ml, whereas FHG110214 produced IAA at a concentration
276 of 0.104 ± 0.021 µg/ml. Instead, without supplementation of Trp, the IAA titres dropped to
277 0.124 ± 0.029 µg/ml (3-fold) and 0.015 ± 0.003 µg/ml (7-fold) in *A. borealis* DSM 23886 and
278 FHG110214, respectively. This production profile is reversed for iP, where Trp supplementation
279 resulted in decreased production for both strains FHG110214 (With Trp: 0.0058 ±0.0012 µg/ml;
280 without Trp: 0.0143 ± 0.0024 µg/ml) and *A. borealis* DSM 23886 (With Trp: 0.005 ±0.0004 µg/ml;
281 Without Trp: 0.0108 ± 0.0008 µg/ml). These production titres are in a comparable range to quantities
282 previously reported for plant-growth-promoting bacteria (PGPB) (51, 52) and, e.g. 10-fold lower
283 compared to those reported for *Pseudomonas*, *Streptomyces*, and *Enterobacter* species, which have
284 been shown to produce 10–150 µg/ml under optimised conditions. The production of the cytokinin iP
285 has not been described so far for the Acidobacteriota phylum. We quantified its production to 0.003
286 µg/ml in the most productive strain of our study. This is in alignment with the literature, which reports,
287 for example, 17.5 pmol/ml (translating to 0.00356 µg/ml) in *Achromobacter xylosoxidans* (53) and
288 lower concentrations such as 0.0003 µg/ml (1.5 nM) in *Paenibacillus polymyxa* (54).

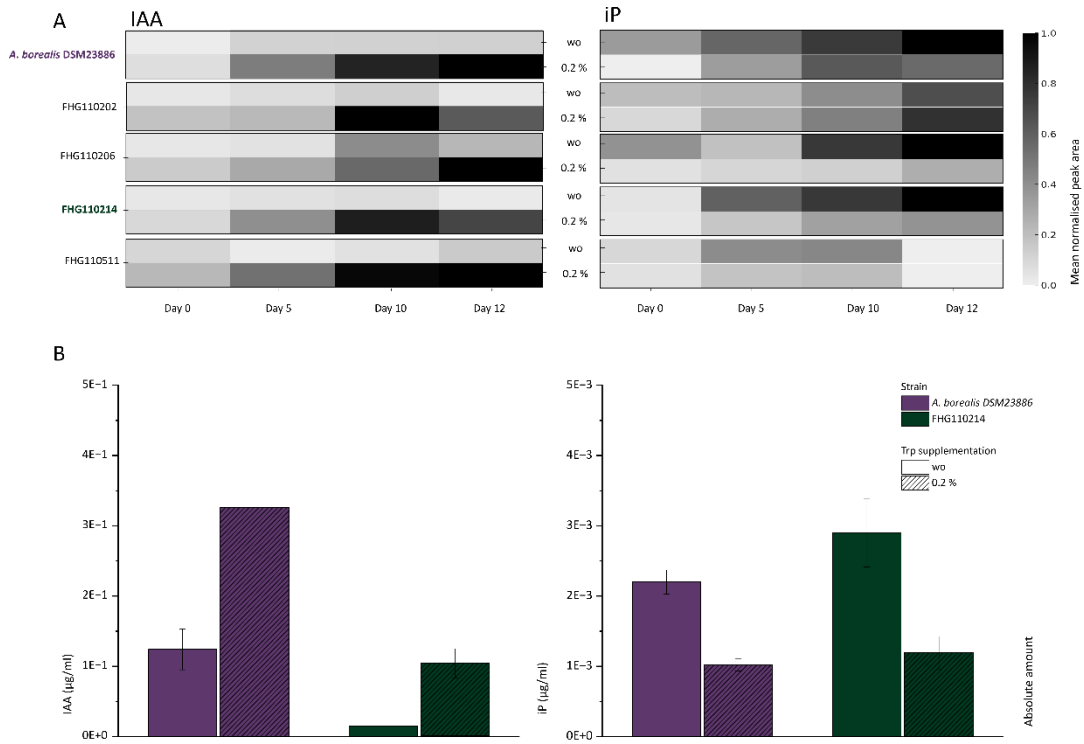

Figure 3: Relative quantification of IAA and iP in FHG *Acidobacteriaceae* and *A. borealis* DSM 23886 as normalised peak area (A) and absolute quantification of these phytohormones in the top producers FHG110214 (iP) and *A. borealis* DSM 23886 (IAA)(B). A Raw peak areas were normalised against the largest peak area within one biological kinetic study for IAA and iP separately. Mean values were calculated and plotted as a heatmap to indicate temporal and dynamic induction patterns between strains and supplementation status. Trp supplementation results in higher IAA production but generally has a negative impact on iP production. This effect is less pronounced in FHG110202 and *A. borealis* DSM 23886. **B** Absolute concentrations were derived from a calibration curve of IAA and iP, correlating peak area with given concentrations. Cultivations were repeated in triplicate, and the average of the calculated concentrations is shown for *A. borealis* DSM 23886 (green) and FHG110214 (purple).

289 Previously, it has been shown that culture broths of IAA-producing *Acidobacteriaceae* promoted root
290 and shoot growth in *Arabidopsis thaliana* (20, 31) and growth and chlorophyll content in duckweed
291 (55). Furthermore, cytokines have also been shown to have a beneficial impact on plant growth and
292 defence response against pathogens and pests (56). To evaluate the plant growth-promoting potential
293 of our extracts, we applied them in concentrations matching the culture concentration on barley
294 seedlings. Additionally, we included a media extract control, as well as IAA and iP at defined
295 concentrations, for testing. Briefly, extracts were spotted into glass vials containing 5 ml SH-medium,
296 and the solvent was evaporated before one barley seed was added per vial. After an initial phase of
297 darkness for germination, a day/night cycle incubation was performed for 6 days (Figure S13).
298 Afterwards, the plants were extracted from the medium, cleaned, and separated into root and shoot
299 before being lyophilised for dry biomass determination (Figure 4A and B). All samples showed a
300 consistently higher biomass if the sample contained Trp. The pure compound controls showed growth
301 comparable to that of the medium with IAA at a concentration of 0.442 µM, resulting in a biomass of
302 11 mg (similar to the medium control containing 0.2% Trp). Compared to the controls, extracts from
303 FHG110214 and *A. borealis* DSM 23886 decreased plant biomass in the shoots (Figure 4A) and roots
304 (Figure 4B) with and without added Trp. However, the addition of Trp to the cultivations decreased
305 the adverse growth effect of the extract itself. Overall, the crude extracts of *A. borealis* and
306 FHG110214 did not significantly promote plant growth of barley seeds in the experimental setup
307 tested. It has been demonstrated that IAA can promote plant growth when bacterial colonies are in
308 direct contact with roots (31). Our experimental setup, in contrast, was executed using cell-free
309 organic extracts to provide a controlled sample. This, however, may not replicate localised, high-

concentration phytohormone effects occurring in natural rhizosphere environments. Furthermore, applying cells or cell-free supernatants may provide further traits, such as enzymes with a beneficial effect on plant growth, not covered by organic extracts. In future studies, live bacterial cultures or co-cultivation systems with plants would provide more ecologically relevant data, albeit with increased challenges associated with cultivation.

Interestingly, our findings, along with those of Kielak *et al*., (31) and Gonçalves *et al*. (20), suggest that phytohormone production is common among Acidobacteriota, particularly among strains isolated from decaying wood or lignocellulosic substrates. This raises intriguing questions about the ecological roles of Acidobacteriota strains producing compounds like IAA and iP in natural systems (57).

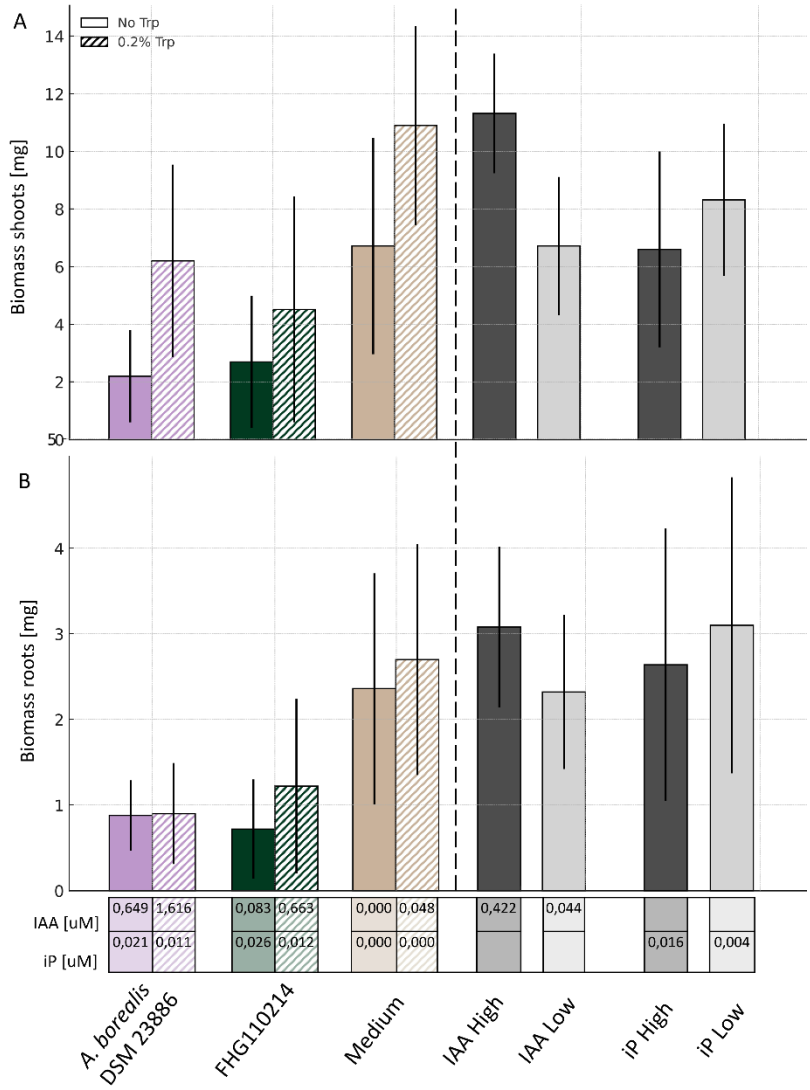

Figure 4: Dry Biomass of barley shoots (A) and roots (B) treated with extracts of strains *A. borealis* DSM 23886 (purple), FHG110214 (green). Striped bars indicate extracts from Trp-supplemented cultivations, while solid bars indicate that extracts were not supplemented with Trp. Media controls (brown), as well as IAA and iP as pure compounds(grey), were also tested. The table indicates the final concentrations of phytohormone applied to the barley seedlings. In general, supplementation with Trp results in increased biomass, especially in the shoots. While pure compound controls show comparable growth to the media control, the strain extracts inhibit plant growth. This negative effect is diminished upon supplementation with Trp, especially in the shoots.

Result 4 – In-Depth Bioinformatic Analysis of PGP Traits in Acidobacteriota and FHG *Acidobacteriaceae*

Taken together, these results confirm that *Acidobacteriaceae* produce phytohormones in relevant amounts, but their role in PGP remains unresolved. Because iP can arise from the degradation of prenylated tRNAs in many bacteria (58), we asked whether *Acidobacteriaceae* also encode dedicated cytokinin pathways (involving lonely guy (LOG) enzymes) and whether these co-occur with additional PGPTs. Furthermore, we were interested in the biosynthetic mechanisms responsible for producing phytohormones. For batch analysis of the 618 genomes previously analysed, we employed a DIAMOND workflow against the PLABASE database (see materials and methods) and summarised hits as coverage (% of PGPT families detected). For the analysis of taxonomic patterns, we aggregated the results by GTDB-Tk family status, only considering acidobacterial families that have been scientifically described or have more than 20 representative genomes available (n = 391, 64.2% of the total dataset). Figure 5 represents the percentage coverage of PGPTs categorised by PLABASE at "level two". Values were hierarchically clustered to visualise similarity between different families and PGPTs. The analysis separated the families into two distinct clusters.

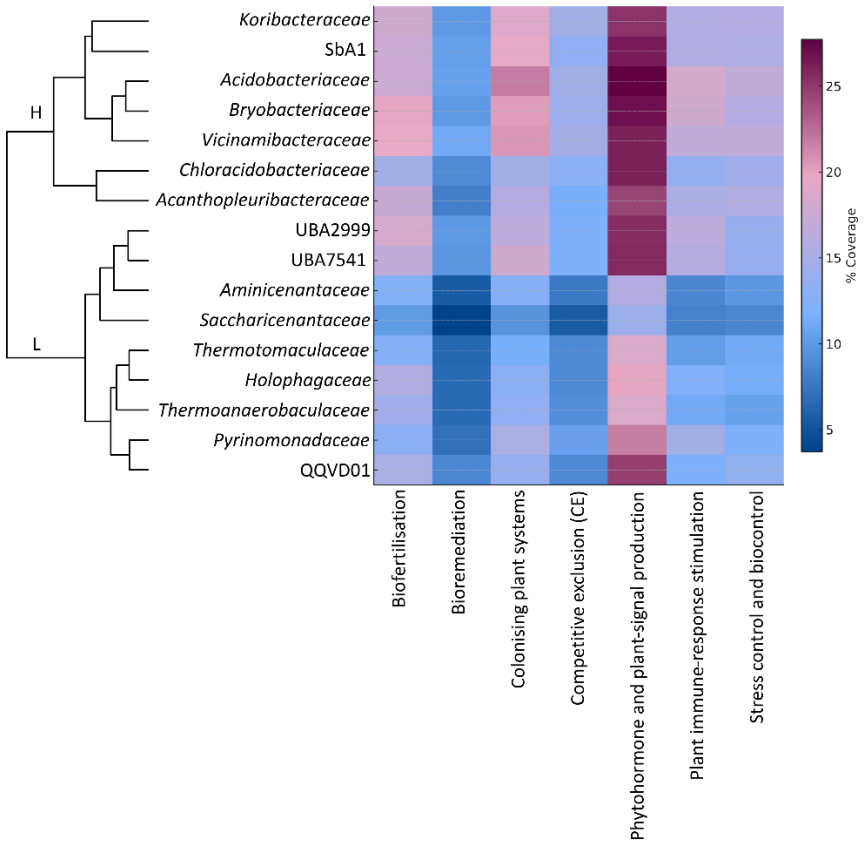

Figure 1: PGPT coverage across Acidobacteriota families. The heatmap displays the mean % coverage of PLABASE PGPT categories (level 2) for families with formal names or more than 20 genomes (n = 16). Coverage values were calculated as the proportion of detected PGPT families per functional category, relative to the total number of families defined in the PLABASE ontology. Rows and columns are hierarchically clustered. Two distinct groups emerge, indicating lower (L, bottom) and higher (H, top) PGPT coverage. The latter exhibits higher potential, particularly in the production of phytohormones and plant signals.

The nine families in the lower-coverage cluster (L) (UBA2999, UBA7541, *Aminicenantaceae*, *Saccharicenantaceae*, *Thermotomaculaceae*, *Holophagaceae*, *Thermoanaerobaculaceae*, *Pyrinomonadaceae*) show a comparatively low average PGPT potential (12.7±1.2%) with uniformly

338 modest values across categories such as biofertilisation: 14.3 ± 1.4%; colonising plant system: 13.7 ±
339 1.4%; stress-control-biocontrol: 11.6 ± 1.0% and especially low bioremediation: 7.2 ± 0.9%. In contrast,
340 families in the higher-coverage cluster H (*Koribacteraceae*, SbA1, *Acidobacteriaceae*,
341 *Bryobacteraceae*, *Vicinamibacteraceae*, *Chloracidobacteriaceae*, *Acanthopleuribacteraceae*) showed
342 consistently higher coverage with representative means of 26.1 ± 2.6% for plant signal production,
343 18.8 ± 2.4% for colonising plant system and 13.7 ± 1.7% competitive exclusion (overall range ~17–26%
344 across categories. Across both clusters, the bioremediation category is underrepresented, while the
345 phytohormone and plant signalling group ranks top among both clusters. Overall, the families of
346 *Bryobacteriaceae*, *Acidobacteriaceae*, and *Vicinamibacteriaceae* exhibit the highest levels of PGPTs.
347 Notably, the *Acidobacteriaceae* perform best in the colonising plant system group (e.g., covering EPS
348 production) and the phytohormone/plant signal production category.

349 We analysed DIAMOND outputs for enzymatic equipment supporting IAA production in our FHG
350 *Acidobacteriaceae* strains. In bacteria, three pathways are described (50): indole-3-pyruvic acid (IPyA),
351 indole-3-acetamide (IAM) and tryptamine (TAM). In the IPyA route, Trp is transaminated to indole-3-
352 pyruvate, decarboxylated to indole-3-acetaldehyde, and oxidised to IAA; the IAM pathway converts
353 Trp to indole-3-acetamide, then hydrolyses it to IAA; the TAM pathway decarboxylates Trp to
354 tryptamine, which is subsequently oxidised via intermediates such as indole-3-acetaldehyde to IAA.
355 All FHG *Acidobacteriaceae* include the key enzymes to synthesise Trp (trpA-E) and terminal enzymes
356 for IAA production, such as an *amiE* homolog for the hydrolysis of indole-3-acetamide, and two
357 aldehyde-dehydrogenases that may catalyse the final step of IAA production in both the TAM and the
358 IPyA pathways. However, the automatic setup did not detect intermediate enzymes. Metabolomics
359 using reference standards identified indole-pyruvic acid (CAS: 392-12-1) upon Trp supplementation,
360 whereas tryptamine (CAS: 61-54-1) was not detected in FHG110202, FHG110214 and *A. borealis*
361 DSM23886. FHG110511 showed neither intermediate. These observations support IPyA as the
362 predominant route over TAM, while IAM remains a possible but unconfirmed option.

363 The production of iP is mediated by two distinct pathways; the t-RNA isopentenyltransferase (IPT)
364 pathway involves the isoprenylation of tRNAs by t-RNA IPTs (*miaA*) and the context-dependent
365 generation of iP through the degradation of these tRNAs (59, 60). The pathway is found ubiquitously
366 in bacteria. Instead, the second pathway is less common and is directly associated with regulated
367 cytokinin output in bacteria, which usually interact with plants. Here, the adenylate IPT modifies
368 adenosine nucleotides using dimethylallyldiphosphate (61), thereby producing iP-like nucleotides
369 further activated by lonely guy (LOG) enzymes (62, 63). Our genomic survey revealed that FHG110511,
370 as well as FHG110214 and *A. borealis* DSM 23886, contain the tRNA-IPT (*miaA*) and accessory genes,
371 while FHG110202 additionally contains a LOG (lonely guy) enzyme. Instead, the adenylate IPT could
372 not be detected in any of the FHG *Acidobacteriaceae*. As indicated by the literature, the *miaA* gene is
373 omnipresent in our acidobacterial dataset, while the LOG enzymes are less present (477/618) but still
374 highly abundant in various acidobacterial classes. Notably, the Trp-responsive iP production aligned
375 with our pathway content. In the strains harbouring the tRNA IDT pathway alone, we determined a
376 reduced iP production upon Trp supplementation. This might be explained by an overall decrease in
377 tRNA turnover due to the high availability of Trp, resulting in a subsequent reduction in global
378 translation and, consequently, lower cytokine release through tRNA degradation mechanisms.
379 Instead, FHG110202, the only inspected strain that harbours a LOG enzyme, does not show a Trp-
380 dependent decrease in iP production, thus possibly less prone to global protein biosynthesis and tRNA
381 turnover rates.

382 We also specifically looked for the presence of vital PGPT factors that could be tested in wet lab
383 experiments. This included plate assays indicating phosphate solubilisation, nitrogen fixation and ACC-

384 deaminase activity. The enzyme ACC deaminase (AcdS) breaks down 1-aminocyclopropane-1-
385 carboxylic acid into ethylene, thereby playing a vital role in the plant defence mechanism. We did not
386 detect *acdS* homologs in our FHG *Acidobacteriaceae* strains. Consistently, we could not detect any
387 growth on plates containing 1-aminocyclopropane-1-carboxylic acid (data not shown). The enzyme
388 AcdS, correlated to PGPT family number 7345, was also searched for in the entire dataset, but was not
389 detected in any strain. The ability to solubilise phosphate from phytate was evaluated on medium
390 containing phytate (data not shown). However, even though we did not detect any growth on agar
391 plates, we identified genes related to phosphate solubilisation through genome mining. *A. borealis*
392 DSM 23886(1.02e-119), FHG110214 (4.91e-107), and FHG110511 (1.57e-148) contained homologs of
393 *appA* (PGPT2560), a phytase known to release Pi from organic phosphorus via a phytase or
394 nucleotidase reaction. We also searched for phytase homologs belonging to PGPT families 2560, 2580,
395 and 2585 in the acidobacterial dataset. Phytases were present in 117 genomes, but only in the classes
396 of *Acidobacteriae* and *Blastocatellia*. The ability to fix nitrogen has been described for the
397 Acidobacteriota before. Recently, Gonçalves *et al.* (20) described the presence of nif clusters in
398 members of the *Holophagaceae* and *Acidobacteriaceae* families. In our genome analysis, we
399 confirmed that members of the *Holophagaceae (Holophagaceae bacterium isolate CTSoil_007)* and
400 *Acidobacteriaceae* (Acidobacteria bacterium isolate SZAS TMP-7) contained nitrogenase clusters
401 encompassing all required *nif* genes A-F (PGPT families PGPT1-30). Besides the *Holophagaceae*, *nif*
402 genes were also detected in *Bryobacteraceae* TMP-7, but not in any of the FHG *Acidobacteriaceae*.

403 Compared to the large-scale metagenomic analysis of Gonçalves *et al.*, our PGPT analysis shows both
404 shared and divergent trends across the acidobacterial families. Some families, such as
405 *Acidobacteriaceae*, *Thermoanaerobaculum*, *Aminicenantesaceae*, *Holophagaceae*, and
406 *Koribacteraceae,* are grouped similarly in terms of their overall equipment, either uniformly high or
407 low; other families show significant discrepancies. Specifically, our results diverge for the families
408 *Bryobacteriaceae, Vicinamibacteraceae, Pyrinomonadaceae, and Chloracidobacteriaceae,* where the
409 PGP potential differs substantially. These differences likely arise from the limited overlap in
410 representative genomes between the two datasets. Overall, 9.2% of our dataset is also covered by the
411 Goncalves dataset. Additionally, our analysis includes seven additional Acidobacteriota families.
412 Notably, the dataset coverage is particularly low for most families with detected discrepancies,
413 including *Bryobacteriaceae* (1/74), *Vicinamibacteraceae* (2/6), and *Pyrinomonadaceae* (2/87). The
414 overlap of the *Chloracidobacteriaceae* (10/14) is relatively high; however, in addition to the dataset
415 composition, methodological differences likely also contribute to the differences. Gonçalves *et al*.
416 focused on 91 curated PGPTs, whereas our genome mining approach utilised the complete PLABASE
417 database, encompassing over 1,300 plant growth-promoting gene families. This broader functional
418 scope may capture additional trait diversity and help explain the differential PGPT evaluation and
419 distribution observed across families.

420 The PGPT profiles of the FHG *Acidobacteriaceae* are consistent with both our broader family-level
421 analysis (Figure 5) and the patterns reported in the large-scale metagenomic study by Goncalves *et al*.
422 (2024). In all cases, *Acidobacteriaceae* show a high frequency of PGPTs, indicating a conserved
423 functional repertoire within this lineage. Notably, Gonçalves *et al*. also identified a similar PGPT
424 pattern in this family, including genes associated with phytohormone biosynthesis and phytase
425 activity. These congruent findings suggest that *Acidobacteriaceae* may play a robust and stable role in
426 plant–microbe interactions across diverse environments.

Result 5 – Effects of Tryptophan on Metabolite Production and Phytopathogen Inhibition

Trp is abundant in the root exudates of many plants, and is described to be used by bacteria to synthesise auxins (64). Indeed, the synthesis of phytohormones by rhizosphere bacteria often depends on the presence of Trp precursors in the root exudates (65). Thus, this metabolic shift might reflect an environmental response of the strains towards the Trp-enriched plant environment (66). To investigate whether supplementation with Trp induces a global metabolic shift or stimulates the production of phytohormones, and to potentially describe the regulated metabolites, we performed time-resolved untargeted metabolomics analysis. Extracts cultivated with and without Trp were analysed with ultra-high-performance liquid chromatography–quadrupole time-of-flight high-resolution mass spectrometry (UHPLC-QTOF-HRMS), and the calculated feature table was filtered to remove features identified as noise. Subsequent principal component analysis (PCA) of log2-transformed feature intensities (Figure S14) revealed that the samples did not exhibit a strict separation by strain or cultivation day, but instead were separated by supplementation status, indicating a broad metabolomic shift associated with Trp supplementation. Furthermore, we observed temporal metabolic shifts that were more distinct for *A. borealis* DSM 23886, especially if supplemented with Trp.

To further investigate Trp-dependent metabolomic responses, we filtered and categorised features based on their presence-absence and fold-change behaviour in response to Trp supplementation. Briefly, features were retained if they were present in both bucketing calculations. Following filtering, feature intensities were compared between the uninduced and induced conditions to derive fold changes. Based on those, we assigned biological categories from “extinguished” to “switched-on”. Individual features were then plotted and coloured to indicate their biological response (Figure S15). The Barcoding plot confirmed the metabolic shift in response to Trp supplementation. We observed differences in media consumption (left side) and changes in features that were clearly strain-dependent (right side). Overall, there is an apparent change in the metabolism indicated by the number of features that change upon Trp supplementation. For *A. borealis* DSM 23886, 165 features are detected on day 14 without Trp, while 684 features (4.1x) are present if Trp is supplemented. The same trend is observed in FHG110214. Here, the feature number increases from 109 (without Trp supplementation) to 337 (3.1x) (with Trp supplementation). We independently verified this result in a second cultivation (Figure S15, bottom half). Here, a similar fold change is observed. While the feature number increases 3.2-fold in *A. borealis* DSM 23886, it exhibits a similar behaviour in FHG110214 (2.8-fold). Those numbers already indicate a strong metabolic activation. This is supported by the fact that, considering all features present under both conditions, 80% of the features are at least lightly upregulated, while 19% are downregulated, and only 1% remain stable.

To further investigate Trp-dependent metabolomic responses considering media and strain-specific features, we classified Trp-activated uptake as referring to features initially present in the medium that were consumed only in Trp-induced cultures. In contrast, Trp-inhibited uptake describes the opposite: features consumed only in uninduced cultures. The rest of the classifications remained the same. Features that were stable in the medium and did not change in intensity were removed from the analysis. Figure 6 (top bar chart) displays the percentage distribution of features across these categories. The “switched on” class accounts for the largest fraction in both strains (*A. borealis* DSM 23886: 56.8%; FHG110214: 45.1%). Specifically, 10.4 and 16.9% of features exhibit an “increased production” profile, while 7.5 and 6.3%, respectively, are “switched off.” Small proportions (below 10%) represent different metabolisation patterns of media components under induced and uninduced conditions.

Given the pronounced metabolic changes observed in Trp-induced extracts, we were encouraged to re-enter our initial bioactivity discovery approach, now particularly testing the generated extracts from FHG110214 and *A. borealis* DSM 23886 for activity against the phytopathogenic fungus *Septoria tritici* MUCL45407, a residue-borne wheat pathogen causing *Septoria tritici* blotch (STB), one of the most significant diseases of wheat (67). By testing our extracts in a microbroth dilution assay, we indeed determined a strong growth-inhibitory effect, exclusively in the samples that underwent Trp supplementation. For the identification of activity-causing compounds, one representative active extract of FHG110214 and *A. borealis* DSM 23886 was microfractionated and re-screened against *S.tritici* MUCL 45407. Based on the molecular formula and the observed MS/MS fragmentation pattern, several Trp-related compounds were dereplicated within the active fractions of both strains, with a confidence level 2 (putatively annotated metabolites (44)). This enabled the annotation of hydroxyglyantrypine (68) as well as malassezindoles A, B (69) and putative yet undescribed derivatives thereof (m/z: 148.1349, 376.1293, 360.1348, 362.1498). Notably, malassezindoles production is known to be strongly dependent on Trp as the sole nitrogen source in their fungal production strains (70). This observation aligns well with our cultivation conditions and experimental setup. However, since the malassezindoles have not been described for bacteria yet, we have expanded our quality control by including regular agar plating, which is conducted concurrently with sampling at the beginning and end of cultivation. Additionally, we continued to perform 16S/18S sequencing from liquid culture samples. Agar plates were incubated for at least 14 days, documented, and routinely inspected using a binocular microscope. Neither measure raised any concerns about handling fungal-contaminated samples. Besides malassezindoles, we annotated the β-carbolines acetyl-beta-carboline, pityriacitrin B (69, 71, 72) and a methylated derivative thereof. Pityriacitrins are produced by fungi and bacteria (73) and recognised for their UV-protective properties (74). Furthermore, the β-carbolines scaffold has been recently reviewed in the context of antifungal activity (75). Indeed, pityriacitrin A, B, and their methyl esters have been described to inhibit fungal growth (73, 76). Furthermore, pityriacitrin B was shown to have protective activity against fungal colonisation of plant hosts (73). In bacterial systems, beta-carboline cores, such as those found in pityriacitrin, are formed via Pictet-Spenglerase enzymes (77–79). Instead, biosynthesis of the Trp-dependent metabolites, closely related to the malassezindoles, has been described for the smut fungus *Ustilago maydis*, where a single enzymatic reaction, catalysed by the enzyme Tam1, is essential for their formation, converting Trp to indolepyruvate (80). Although the biosynthetic pathways for these compounds have not been elucidated in bacteria, a similar mechanism can be inferred. However, a BLAST search for analogous proteins within our acidobacterial genome dataset did not yield any significant hits. An additional signal observed in the active fraction, co-eluting with malassezindoles under the applied chromatographic conditions, suggested the presence of a peptide, with an m/z value of 519.1655 [M+H]+ corresponding to the molecular formula $C_{30}H_{22}N_4O_5$.

We focused our isolation efforts on compounds previously reported to exhibit antifungal properties. Preparative and semi-preparative isolation methods were employed on the fractions containing malassezindoles and their derivatives. Two compounds were purified, and their structures were elucidated by NMR analysis in DMSO-d_6, employing ^{1}H, ^{13}C, COSY, HSQC, HMBC, TOCSY, ROESY and NOESY measurements (Table S3-4). Compound **1** ($C_{21}H_{13}N_3O_3$) was identified as pityriacitrin B, while compound **2** ($C_{22}H_{15}N_3O_3$) was determined to be its methyl ester. The spectroscopic data for both compounds were consistent with literature reports (72, 81). Detailed ^{1}H and ^{13}C NMR data, as well as key COSY, ROESY and HMBC correlations, are summarised in the Supporting Information (Tables S2–S3).To examine the features previously identified to be bioactive, we mapped them onto our categorised feature dataset. This allowed us to assess which metabolic response classes these

metabolites belong to. Additionally, we explored other Trp-dependent masses by molecular networking, aiming to identify novel or derivative compounds using database annotations.

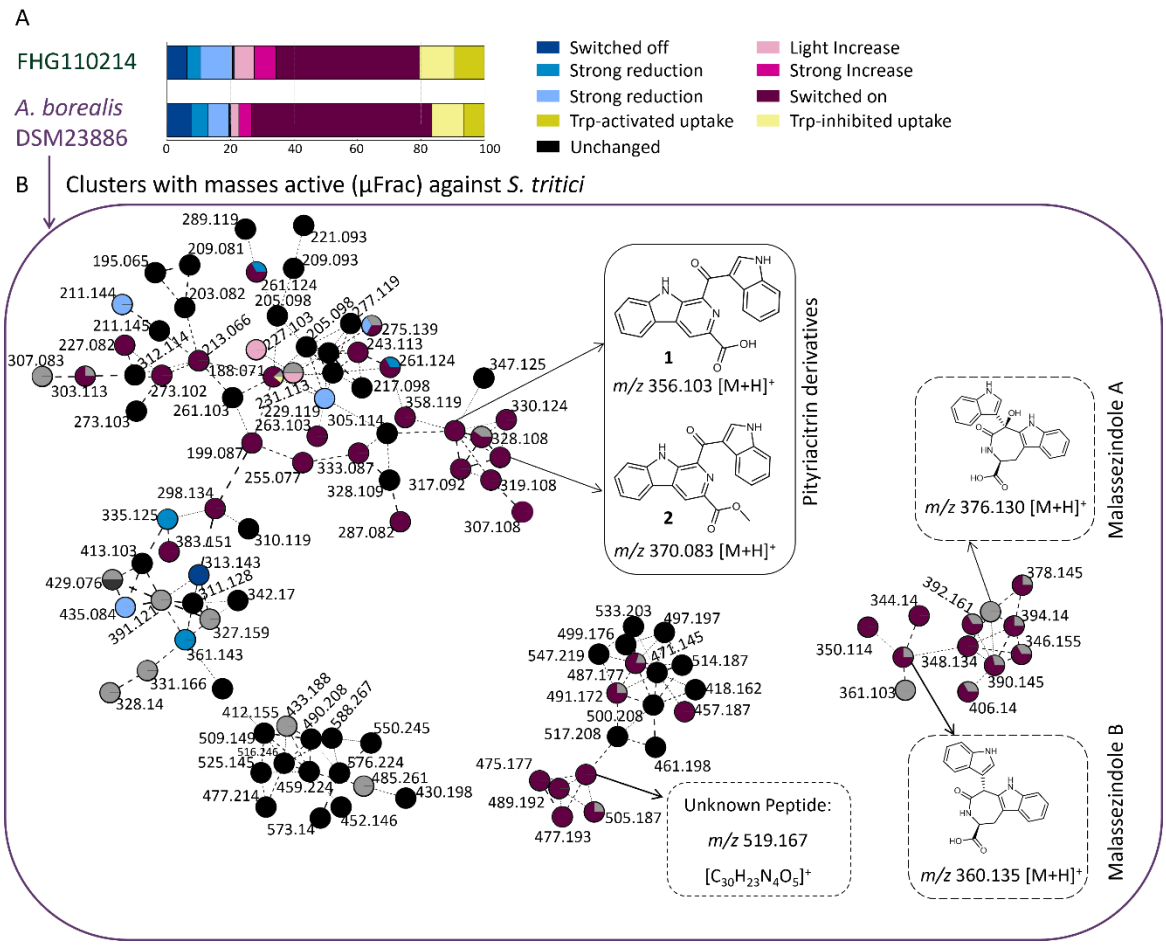

Figure 2: Overall metabolic response of cultivation with Trp in strains FHG110214 and *A. borealis* DSM 23886 (A). Molecular network of masses active against *S. tritici* MUCL 45407 as detected by µFrac-coupled screening of *A. borealis* DSM 23886 extracts (B). (A) After feature detection, the relative presence of masses with and without Trp was compared for categorisation. Categories were defined as follows: "switched-off" (dark-blue, no feature detected upon Trp supplementation) and "switched-on" (dark-red, Feature only present upon Trp supplementation). Media components that were metabolised differently upon Trp supplementation are shown in yellow. (B)Molecular Networking of MS/MS data generated from a Trp-induced *A. borealis* DSM 23886 culture, limited to clusters containing masses that showed antifungal activity against *S. tritici* MUCL 45407. Active masses were all specifically "switched on" when supplemented with Trp. While some of them remained unknown (e.g. 519.167m/z peptide), others were dereplicated by comparison with database standards (malassezindole A,B) or isolated and structure elucidated(pityriacitrin B and pityriacitrin B methyl ester).

The observed changes in activity profiles and the Trp-dependent modulation of extracts underscore the impact of Trp supplementation on the production of specific, bioactivity-causing compounds. Having already linked several of these induced features to bioactivity through microfractionation, we next turned to molecular networking to explore their structural context within the overall metabolome. This approach enabled us to visualise whether the bioactive compounds belong to larger molecular families, identify structurally related analogues, and determine whether induction leads to the coordinated activation of specific metabolic clusters. By integrating activity data with MS/MS-based network topology, we aimed to prioritise entire subnetworks of interest and assess how broadly Trp supplementation influences distinct chemical families across strains.

Acidobacteriota often dominate soil bacterial communities, particularly in acidic and oligotrophic environments, yet their functional roles remain underexplored. Our findings contribute to growing

533 evidence that members of this phylum possess underestimated biosynthetic and ecological potential,
534 including the ability to produce phytohormones and possibly bioactive metabolites with the potential
535 to antagonise fungal growth.

536 Beyond our cultivated FHG *Acidobacteriaceae*, genome-mining of 618 high-quality Acidobacteriota
537 genomes offers a complementary perspective to the large-scale MAG-based analysis by
538 Gonçalves *et al*. (2024), which analysed 758 MAGs. Both studies identify *Acidobacteriaceae*,
539 *Bryobacteriaceae*, and *Koribacteraceae* as families with enriched PGPT potential, while families such
540 as *Holophagaceae* and *Vicinamibacteraceae* appear comparatively under-equipped. However,
541 notable discrepancies emerged, likely reflecting differences in the underlying datasets and the
542 methodological approach.

543 Despite the current technical limitations, exploring Acidobacteriota as sources of novel bioactive
544 compounds or as contributors to plant–soil health remains a promising avenue. A considerable
545 limitation, however, is their challenging growth in laboratory settings. If obtained as isolates, their
546 total cell biomass remained low, even when using optimised media conditions, and some strains even
547 show aggregated growth forms. Given the intriguing biosynthetic potential predicted from the
548 genome, more efforts are needed to characterise and exploit this phylum, including, for example, the
549 development of genetic tools for in situ activation, overexpression, and deletion of specific genes, as
550 well as the establishment of a genetically tractable heterologous expression system in
551 Acidobacteriota-hosts. Together, this could lead to a better understanding and utilisation of
552 Acidobacteriota, aiming to discover new methods for their role in sustainable agriculture,
553 bioremediation, and natural product discovery.

554 Methods

555 Microbial cultivation of acidobacterial strains

556 Acidobacterial strains were routinely cultivated in R2A Medium (R2A Broth, HIMEDIA, Maharashtra,
557 India) buffered with MES-hydrate(2-(N-Morpholino)ethanesulfonic acid hydrate, CAS: 1266615-59-1)
558 (1.95 g/l) at pH 6.0. Cultures were incubated at 28°C with 75 rpm. To sustain healthy and continuous
559 growth, 10% of the 7-day-old preculture (30 ml in 100 ml Erlenmeyer flask) was used to inoculate the
560 main cultures (100 ml in 300 ml Erlenmeyer flasks). For quality control, we transferred 100 µl after
561 each inoculation or sampling step to an R2A-MES-buffered agar plate to observe colony morphologies
562 and identify the growth of contaminant microorganisms. Additionally, we performed 16S rRNA gene
563 amplification testing with primer pair E8F (50-GAG TTT GAT CCT GGC TCA G-30) and 1492R (50-ACG
564 GYT ACC TTG TTA CGA CTT-30) (Lane, 1991). For the OSMAC cultivation approach, we performed 24-
565 well-scale and Erlenmeyer flask-scale cultivation. We prepared forty 24-well Duetz system plates with
566 20 different media (each medium 4 ml) and autoclaved the plates before inoculation (10%) with a
567 preculture grown for 14 days. Applied media were diluted medium 5254 (82)(2 g soluble starch, 2 g
568 glycerol, 0.5 g corn steep liquor 1 g peptone, 0.4 g yeast extract, 0.2 g NaCl; pH 5.5, buffered with 1.95
569 g/L MES), HD (0.5 g casein peptone, 0.1 g glucose, 0.25 g yeast extract; pH 5.0, unbuffered; DSMZ ID
570 1135), and PSYA 5 (26)(1.8 g KH_2PO_4, 0.2 g $MgSO_4$ x $7H_2O$, 1 g yeast extract; optionally with addition
571 of sucrose at 0.5% or 3%; pH 5.0, unbuffered) as well as a diversity of VL55-based and R2A-based (1-
572 fold, 2-fold, 4-fold) media generated by optional addition of different carbon sources (Pektin, GlcNAc
573 – 0.05%; Xylan, Cellobiose – 0.5%; and Sucrose 3%; applied to 2-fold R2A)(Table S2) (25, 39).
574 Furthermore, as a surface attachment enabling strategy, we added ceramic beads (hollow cylinders;
575 3 pcs/well plus 4 ml of media), quartz beads (round; 10 pcs/well plus 4 ml of media), or solidified the
576 respective medium using 0.8% phytagel. The plates were incubated at 28°C, shaking at 120 rpm or
577 with manual shaking once per day. Cultivation in a 300 ml Erlenmeyer flask was executed in 100 mL

578 media by inoculation (10%) with a preculture grown for 7 days. The cultures were incubated at 28°C
579 for 14 days with or without shaking at 75 rpm. We added 20 g of ceramic beads (Eheim mech) to non-
580 shaking cultures. After cultivation, cultures were frozen, freeze-dried and extracted (see below).

581 For Trp-induced kinetic studies, we used a 1.2-fold concentrated R2A medium buffered with 2-(*N*-
582 morpholino)ethanesulfonic acid (MES) at a pH of 6.0, which was supplemented in a 4:1 ratio with 1%
583 sterile-filtered Trp (CAS 73-22-3) to a final concentration of 0.2% Trp and a 1-fold concentrated
584 medium. Kinetic studies were performed in 300 ml flasks at least in duplicates. For sample collection,
585 we transferred 4 ml of culture to 24-deep-well plates for further processing. In parallel, the remaining
586 culture sample was used for quality control by agar plating (R2A-MES, pH 6.0) and 16S rDNA PCR. After
587 the final harvest day, the 24-well plates were freeze-dried and extracted using methanol (SI-extended
588 methods and results).

589 Bioassays

590 Antimicrobial Screenings of crude extracts were performed using microplate broth dilution assays at
591 the final assay concentration of 0.25-fold, 0.5-fold, one-fold and two-fold (in relation to the culture
592 volume) against bacteria and fungi (*Escherichia coli* ATCC 35218, *Bacillus subtilis* DSM 10,
593 *Mycobacterium smegmatis* ATCC 607, *Candida albicans* FH 2173 and *Septoria tritici* MUCL 45407) as
594 described previously (39). Crude extracts showing at least 70% growth inhibition were considered
595 bioactive and were subjected to microfractionation for dereplication of bioactivity-causing
596 metabolites (39). Testing of crude extracts on barley seedlings was performed in glass vials filled with
597 5 ml of SH medium, inoculated with one surface-disinfected barley seed per vial (SI-extended methods
598 and results).

599 Creation and Curation of the Acidobacteriota Genome Dataset

600 As of March 2023, Acidobacteriota assemblies matching our selection criteria (NCBI:txid, filter: RefSeq
601 annotation) were retrieved from NCBI in .gbff file format. In addition, four Acidobacteriota assemblies,
602 from strains isolated from termite nest material (FHG110202, FHG110214), soil (FHG110511) and a
603 genome generated for *A. borealis* DSM 23886 complemented the dataset (n = 1425). Genome
604 assemblies were selected based on their completeness and contamination using CheckM2(40). Only
605 high-quality genome assemblies defined by MIMAG (41) evaluation criteria demonstrating 90-100%
606 completeness and 0-5% contamination were retained for further evaluation (n = 648). For this,
607 redundancies and taxonomic affiliation were checked by GTDB-Tk (42). In total, 618 curated genome
608 assemblies were processed for metadata evaluation, BGC potential, and PGPT mining (SI-extended
609 methods and results for details). To correlate the genomic data to the taxonomic affiliation, a whole-
610 genome sequence-based phylogenetic tree of the GTDB-generated multiple-sequence alignment file
611 was visualised using iTOL v4 (45).

612 Genomic Analysis of PGPT Traits

613 The coding sequences from the previously described genomic dataset were extracted using a custom
614 Python pipeline built with BioPython (SeqIO). To generate FASTA documents for further processing,
615 we retrieved the gene name, product description and translated protein sequence for each CDS. For
616 pre-existing FASTA files, the extraction of CDSs can be skipped. To document the number of CDSs
617 extracted per genome, a log file was generated. The PLABASE PGPT database (83)
618 (PGPT_BASE_nr_Aug2021n_ul_1.dmnd) was used as a reference for a similarity search against the
619 extracted protein sequences using DIAMOND v2. The script supports various sensitivity modes,
620 enabling users to select the most suitable mode based on their specific input. The parameters and
621 applied evaluation thresholds used in this study are described in the Extended Methods and Results
622 section of the supplementary information.

Mass spectrometry

Ultra-high-performance liquid chromatography (UHPLC) coupled with quadrupole time-of-flight (QTOF) high-resolution mass spectrometry (HR-MS) and tandem MS (MS/MS) was performed using an Agilent 1290 Infinity LC system connected to a maXis II QTOF mass spectrometer (Bruker Daltonics) equipped with an electrospray ionisation (ESI) source. Separation of samples was achieved on an Acquity UPLC BEH C18 column (130 Å pore size, 1.7 µm particle size, 2.1 × 100 mm) fitted with a matching pre-column (2.1 × 5 mm, 1.7 µm, 130 Å) at a temperature of 45°C. Chromatographic separation was achieved using a linear gradient elution of solvent A (water with 0.1% formic acid) and solvent B (acetonitrile with 0.1% formic acid) at a constant flow rate of 0.6 ml/min. The gradient program was as follows: 95% A at 0.00–0.30 min, gradually decreasing to 4.75% A by 18.00 min, then to 0% A at 18.10 min, held until 22.50 min, returned to 95% A at 22.60 min, and equilibrated until 25.00 min. Mass spectra were recorded in positive mode over a mass range of m/z 50–2000 with a spectra rate of 1 Hz. MS/MS acquisition was performed at a 6 Hz scan rate, targeting the top five most intense ions per full mass spectrum for collision-induced dissociation (CID) using nitrogen, as per the table published by Eichberg *et al.* (84). Precursors were excluded after two spectra, with a release duration of 0.5 min, and re-evaluated if their signal intensity increased by ≥1.5-fold. All data analysis was performed with DataAnalysis 4.4 (Bruker, Billerica, MA, USA).

Chemotype-barcoding matrix, Multivariate analysis and statistics

Raw data processing was performed using DataAnalysis 5.2 (Bruker) as previously published, and the complete data set was copied and processed with both line spectra thresholds (here: 5,000 and 10,000) (85). Bucketing was performed on both sets at the same time, resulting in one table containing all buckets deemed identical for every sample (under both thresholds) and by applying the data curation measures as described in the extended methods and results of the supplementary information. This analysis revealed a final table of 219 samples with 3,092 buckets (OSMAC) and 48 samples with 2,759 buckets (Trp-Induction), which were used for the respective barcode generation and for categorising. The generated bucket tables were used as (i) a binary presence/absence matrix (result 1) or (ii) a quantitative intensity matrix (result 5). For PCoA on the binary matrix, (i) Jaccard dissimilarities were computed (skbio.diversity.beta_diversity, metric="jaccard"), and PCoA (skbio.stats.ordination.pcoa) was done using scikit-bio (v0.7.0). PERMANOVA (skbio.stats.distance.permanova) assessed group differences with 999 permutations. We tested the effects of medium, cultivation size (small-scale vs. large-scale), and bead condition (Quartz/Ceramic/None) in a small-scale subset. For PCA on quantitative data (ii), we log2-transformed peak area intensities using scikit-learn (v1.3) in Python. Before PCA, undetected features were defined as zero, and samples were normalised to the injection volume wherever indicated. All visualisations were generated using Matplotlib, with attributes changed based on metadata information through shape, colour, and border style to reflect replicates and experimental conditions.

Compound Isolation

The crude extract was dissolved in 10% MeOH to perform SPE utilising a 2 L column packed with Amberlite XAD-16 N and step gradient elution of 10%, 20%, 40%, 60%, 80%, and 100% MeOH. Based on LC-MS analysis, several fractions containing the compounds of interest were combined and evaporated to dryness. During isolation, semi-preparative and preparative HPLC were performed on Agilent 1100 HPLC systems equipped with external Gilson fraction collectors using H2O + 0.1% FA and ACN + 0.1% FA as mobile phases. Final purification was achieved by UPLC fractionation using the chromatographic method described in the UPLC-MS section, with fraction collection of 16 seconds per fraction, starting directly after injection.

Structure elucidation by NMR

NMR spectra were recorded on a Bruker AVANCE III HD 700 MHz spectrometer operating at ^{1}H frequency of 700 MHz and a ^{13}C-carbon frequency of 140 MHz. The instrument was equipped with a 5 mm TCI cryo probe head. COSY, TOCSY, ROESY, NOESY, HSQC, and HMBC experiments were recorded using standard pulse programs. All isolated samples were measured in DMSO-d6. Chemical shifts were referenced to the solvent signals (^{1}H: 2.50 ppm, ^{13}C: 39.5 ppm)

References

1. Jones RT, Robeson MS, Lauber CL, Hamady M, Knight R, Fierer N. 2009. A comprehensive survey of soil acidobacterial diversity using pyrosequencing and clone library analyses. The ISME Journal 3:442–453.

2. Koch IH, Gich F, Dunfield PF, Overmann J. 2008. Edaphobacter modestus gen. nov., sp. nov., and Edaphobacter aggregans sp. nov., acidobacteria isolated from alpine and forest soils. International Journal of Systematic and Evolutionary Microbiology 58:1114–1122.

3. Eichorst SA, Breznak JA, Schmidt TM. 2007. Isolation and Characterization of Soil Bacteria That Define Terriglobus gen. nov., in the Phylum Acidobacteria. Appl Environ Microbiol 73:2708–2717.

4. Flieder M, Buongiorno J, Herbold CW, Hausmann B, Rattei T, Lloyd KG, Loy A, Wasmund K. 2021. Novel taxa of Acidobacteriota implicated in seafloor sulfur cycling. ISME J 1–22.

5. Mehta-Kolte MG, Bond DR. 2012. Geothrix fermentans Secretes Two Different Redox-Active Compounds To Utilize Electron Acceptors across a Wide Range of Redox Potentials. Appl Environ Microbiol 78:6987–6995.

6. Pankratov TA, Dedysh SN. 2010. Granulicella paludicola gen. nov., sp. nov., Granulicella pectinivorans sp. nov., Granulicella aggregans sp. nov. and Granulicella rosea sp. nov., acidophilic, polymer-degrading acidobacteria from Sphagnum peat bogs. International Journal of Systematic and Evolutionary Microbiology, 60:2951–2959.

7. Belova SE, Ravin NV, Pankratov TA, Rakitin AL, Ivanova AA, Beletsky AV, Mardanov AV, Sinninghe Damsté JS, Dedysh SN. 2018. Hydrolytic Capabilities as a Key to Environmental Success: Chitinolytic and Cellulolytic Acidobacteria From Acidic Sub-arctic Soils and Boreal Peatlands. Front Microbiol 9.

8. Sipes K, Buongiorno J, Steen AD, Abramov AA, Abuah C, Peters SL, Gianonne RJ, Hettich RL, Boike J, Garcia SL, Vishnivetskaya TA, Lloyd KG. 2024. Depth-specific distribution of bacterial MAGs in permafrost active layer in Ny Ålesund, Svalbard (79°N). Systematic and Applied Microbiology 47:126544.

9. Kishimoto N, Kosako Y, Tano T. 1991. Acidobacterium capsulatum gen. nov., sp. nov.: An acidophilic chemoorganotrophic bacterium containing menaquinone from acidic mineral environment. Current Microbiology 22:1–7.

10. Ludwig W, Bauer SH, Bauer M, Held I, Kirchhof G, Schulze R, Huber I, Spring S, Hartmann A, Schleifer KH. 1997. Detection and in situ identification of representatives of a widely distributed new bacterial phylum. FEMS Microbiology Letters 153:181–190.

11. Quaiser A, Ochsenreiter T, Lanz C, Schuster SC, Treusch AH, Eck J, Schleper C. 2003. Acidobacteria form a coherent but highly diverse group within the bacterial domain: evidence from environmental genomics. Molecular Microbiology 50:563–575.

12. Dedysh SN, Yilmaz P. 2018. Refining the taxonomic structure of the phylum Acidobacteria. International Journal of Systematic and Evolutionary Microbiology 68:3796–3806.

13. Ward NL, Challacombe JF, Janssen PH, Henrissat B, Coutinho PM, Wu M, Xie G, Haft DH, Sait M, Badger J, Barabote RD, Bradley B, Brettin TS, Brinkac LM, Bruce D, Creasy T, Daugherty SC, Davidsen TM, DeBoy RT, Detter JC, Dodson RJ, Durkin AS, Ganapathy A, Gwinn-Giglio M, Han CS, Khouri H, Kiss H, Kothari SP, Madupu R, Nelson KE, Nelson WC, Paulsen I, Penn K, Ren Q, Rosovitz MJ, Selengut JD, Shrivastava S, Sullivan SA, Tapia R, Thompson LS, Watkins KL, Yang Q, Yu C, Zafar N, Zhou L, Kuske CR. 2009. Three Genomes from the Phylum Acidobacteria Provide Insight into the Lifestyles of These Microorganisms in Soils. Appl Environ Microbiol 75:2046–2056.

14. Lee S-H, Ka J-O, Cho J-C. 2008. Members of the phylum Acidobacteria are dominant and metabolically active in rhizosphere soil. FEMS Microbiol Lett 285:263–269.

15. Dyksma S, Pester M. 2023. Oxygen respiration and polysaccharide degradation by a sulfate-reducing acidobacterium. Nat Commun 14:6337.

16. Foesel BU, Rohde M, Overmann J. 2013. Blastocatella fastidiosa gen. nov., sp. nov., isolated from semiarid savanna soil – The first described species of Acidobacteria subdivision 4. Systematic and Applied Microbiology 36:82–89.

17. Hausmann B, Pelikan C, Herbold CW, Köstlbacher S, Albertsen M, Eichorst SA, Rio TG del, Huemer M, Nielsen PH, Rattei T, Stingl U, Tringe SG, Trojan D, Wentrup C, Woebken D, Pester M, Loy A. 2018. Peatland Acidobacteria with a dissimilatory sulfur metabolism. ISME J 12:1729–1742.

18. Reji L, Zhang X. 2022. Genome-Resolved Metagenomics Informs the Functional Ecology of Uncultured Acidobacteria in Redox Oscillated Sphagnum Peat. mSystems 7:e00055-22.

19. Giguere AT, Eichorst SA, Meier DV, Herbold CW, Richter A, Greening C, Woebken D. 2021. Acidobacteria are active and abundant members of diverse atmospheric H2-oxidizing communities detected in temperate soils. ISME J 15:363–376.

20. Gonçalves OS, Fernandes AS, Tupy SM, Ferreira TG, Almeida LN, Creevey CJ, Santana MF. 2024. Insights into plant interactions and the biogeochemical role of the globally widespread Acidobacteriota phylum. Soil Biology and Biochemistry 192:109369.

21. Parsley LC, Linneman J, Goode AM, Becklund K, George I, Goodman RM, Lopanik NB, Liles MR. 2011. Polyketide synthase pathways identified from a metagenomic library are derived from soil Acidobacteria. FEMS Microbiology Ecology 78:176–187.

22. Crits-Christoph A, Diamond S, Butterfield CN, Thomas BC, Banfield JF. 2018. Novel soil bacteria possess diverse genes for secondary metabolite biosynthesis. Nature 558:440–444.

23. McReynolds E, Elshahed MS, Youssef NH. 2025. An ecological-evolutionary perspective on the genomic diversity and habitat preferences of the Acidobacteriota. Microbial Genomics 11:001344.

745 24. Leopold-Messer S, Chepkirui C, Mabesoone MFJ, Meyer J, Paoli L, Sunagawa S, Uria AR,
746 Wakimoto T, Piel J. 2023. Animal-associated marine Acidobacteria with a rich natural-product
747 repertoire. Chem 9:3696–3713.

748 25. Oberpaul M, Zumkeller CM, Culver T, Spohn M, Mihajlovic S, Leis B, Glaeser SP, Plarre R,
749 McMahon DP, Hammann P, Schäberle TF, Glaeser J, Vilcinskas A. 2020. High-throughput
750 cultivation for the selective isolation of Acidobacteria from termite nests. Front Microbiol 11.

751 26. Campanharo JC, Kielak AM, Castellane TCL, Kuramae EE, Lemos EG de M. 2016. Optimized
752 medium culture for Acidobacteria subdivision 1 strains. FEMS Microbiology Letters 363:fnw245.

753 27. Sait M, Hugenholtz P, Janssen PH. 2002. Cultivation of globally distributed soil bacteria from
754 phylogenetic lineages previously only detected in cultivation-independent surveys.
755 Environmental Microbiology 4:654–666.

756 28. Kuske CR, Barns SM, Busch JD. 1997. Diverse uncultivated bacterial groups from soils of the arid
757 southwestern United States that are present in many geographic regions. Applied and
758 Environmental Microbiology 63:3614–3621.

759 29. Felske A, De Vos WM, Akkermans ADL. 2000. Spatial distribution of 16S rRNA levels from
760 uncultured acidobacteria in soil. Lett Appl Microbiol 31:118–122.

761 30. Eichorst SA, Kuske CR, Schmidt TM. 2011. Influence of Plant Polymers on the Distribution and
762 Cultivation of Bacteria in the Phylum Acidobacteria. Applied and Environmental Microbiology
763 77:586–596.

764 31. Kielak AM, Cipriano MAP, Kuramae EE. 2016. Acidobacteria strains from subdivision 1 act as
765 plant growth-promoting bacteria. Arch Microbiol 198:987–993.

766 32. Damsté JSS, Rijpstra WIC, Dedysh SN, Foesel BU, Villanueva L. 2017. Pheno- and Genotyping of
767 Hopanoid Production in Acidobacteria. Front Microbiol 8.

768 33. Kielak AM, Castellane TCL, Campanharo JC, Colnago LA, Costa OYA, Corradi da Silva ML, van Veen
769 JA, Lemos EGM, Kuramae EE. 2017. Characterization of novel Acidobacteria exopolysaccharides
770 with potential industrial and ecological applications. Sci Rep 7:41193.

771 34. Kalam S, Basu A, Ahmad I, Sayyed RZ, El-Enshasy HA, Dailin DJ, Suriani NL. 2020. Recent
772 Understanding of Soil Acidobacteria and Their Ecological Significance: A Critical Review. Frontiers
773 in Microbiology 11:2712.

774 35. Trojan D, García-Robledo E, Hausmann B, Revsbech NP, Woebken D, Eichorst SA. 2024. A respiro-
775 fermentative strategy to survive nanoxia in Acidobacterium capsulatum. FEMS Microbiol Ecol
776 100:fiae152.

777 36. Costa OYA, Zerillo MM, Zühlke D, Kielak AM, Pijl A, Riedel K, Kuramae EE. 2020. Responses of
778 Acidobacteria Granulicella sp. WH15 to High Carbon Revealed by Integrated Omics Analyses.
779 Microorganisms 8:244.

780 37. Halamka TA, Garcia A, Evans TW, Schubert S, Younkin A, Hinrichs K-U, Kopf S. 2024. Occurrence
781 of ceramides in the Acidobacterium Solibacter usitatus: implications for bacterial physiology and
782 sphingolipids in soils. Front Geochem 2.

783 38. Sinninghe Damsté JS, Rijpstra WIC, Hopmans EC, Weijers JWH, Foesel BU, Overmann J, Dedysh
784 SN. 2011. 13,16-Dimethyl Octacosanedioic Acid (iso-Diabolic Acid), a Common Membrane-
785 Spanning Lipid of Acidobacteria Subdivisions 1 and 3. Applied and Environmental Microbiology
786 77:4147–4154.

787 39. Oberpaul M, Brinkmann S, Marner M, Mihajlovic S, Leis B, Patras MA, Hartwig C, Vilcinskas A,
788 Hammann PE, Schäberle TF, Spohn M, Glaeser J. 2022. Combination of high-throughput
789 microfluidics and FACS technologies to leverage the numbers game in natural product discovery.
790 Microbial Biotechnology 15:415–430.

791 40. Chklovski A, Parks DH, Woodcroft BJ, Tyson GW. 2023. CheckM2: a rapid, scalable and accurate
792 tool for assessing microbial genome quality using machine learning. Nat Methods 20:1203–1212.

793 41. Bowers RM, Kyrpides NC, Stepanauskas R, Harmon-Smith M, Doud D, Reddy TBK, Schulz F, Jarett
794 J, Rivers AR, Eloe-Fadrosh EA, Tringe SG, Ivanova NN, Copeland A, Clum A, Becraft ED,
795 Malmstrom RR, Birren B, Podar M, Bork P, Weinstock GM, Garrity GM, Dodsworth JA, Yooseph
796 S, Sutton G, Glöckner FO, Gilbert JA, Nelson WC, Hallam SJ, Jungbluth SP, Ettema TJG, Tighe S,
797 Konstantinidis KT, Liu W-T, Baker BJ, Rattei T, Eisen JA, Hedlund B, McMahon KD, Fierer N, Knight
798 R, Finn R, Cochrane G, Karsch-Mizrachi I, Tyson GW, Rinke C, Lapidus A, Meyer F, Yilmaz P, Parks
799 DH, Murat Eren A, Schriml L, Banfield JF, Hugenholtz P, Woyke T. 2017. Minimum information
800 about a single amplified genome (MISAG) and a metagenome-assembled genome (MIMAG) of
801 bacteria and archaea. Nat Biotechnol 35:725–731.

802 42. Parks DH, Chuvochina M, Rinke C, Mussig AJ, Chaumeil P-A, Hugenholtz P. 2022. GTDB: an
803 ongoing census of bacterial and archaeal diversity through a phylogenetically consistent, rank
804 normalized and complete genome-based taxonomy. Nucleic Acids Research 50:D785–D794.

805 43. Bode HB, Bethe B, Höfs R, Zeeck A. 2002. Big effects from small changes: possible ways to explore
806 nature's chemical diversity. Chembiochem 3:619–627.

807 44. Sumner LW, Amberg A, Barrett D, Beale MH, Beger R, Daykin CA, Fan TW-M, Fiehn O, Goodacre
808 R, Griffin JL, Hankemeier T, Hardy N, Harnly J, Higashi R, Kopka J, Lane AN, Lindon JC, Marriott P,
809 Nicholls AW, Reily MD, Thaden JJ, Viant MR. 2007. Proposed minimum reporting standards for
810 chemical analysis Chemical Analysis Working Group (CAWG) Metabolomics Standards Initiative
811 (MSI). Metabolomics 3:211–221.

812 45. Letunic I, Bork P. 2019. Interactive Tree Of Life (iTOL) v4: recent updates and new developments.
813 Nucleic Acids Res 47:W256–W259.

814 46. Blin K, Shaw S, Kloosterman AM, Charlop-Powers Z, van Wezel GP, Medema MH, Weber T. 2021.
815 antiSMASH 6.0: improving cluster detection and comparison capabilities. Nucleic Acids Res
816 49:W29–W35.

817 47. Navarro-Muñoz JC, Selem-Mojica N, Mullowney MW, Kautsar SA, Tryon JH, Parkinson EI, De Los
818 Santos ELC, Yeong M, Cruz-Morales P, Abubucker S, Roeters A, Lokhorst W, Fernandez-Guerra
819 A, Cappelini LTD, Goering AW, Thomson RJ, Metcalf WW, Kelleher NL, Barona-Gomez F, Medema
820 MH. 2020. A computational framework to explore large-scale biosynthetic diversity. Nat Chem
821 Biol 16:60–68.

822 48. Gu G, Smith L, Liu A, Lu S-E. 2011. Genetic and Biochemical Map for the Biosynthesis of
823 Occidiofungin, an Antifungal Produced by Burkholderia contaminans Strain MS14 ▿. Appl
824 Environ Microbiol 77:6189–6198.

825 49. Cothrell A, Cao K, Bonasera R, Tenorio A, Orugunty R, Smith L. 2023. Intravaginal Gel for
826 Sustained Delivery of Occidiofungin and Long-Lasting Antifungal Effects. Gels 9:787.

827 50. Spaepen S, Vanderleyden J, Remans R. 2007. Indole-3-acetic acid in microbial and
828 microorganism-plant signaling. FEMS Microbiology Reviews 31:425–448.

829 51. Schmidt CS, Mrnka L, Frantík T, Lovecká P, Vosátka M. 2018. Plant growth promotion of
830 Miscanthus × giganteus by endophytic bacteria and fungi on non-polluted and polluted soils.
831 World J Microbiol Biotechnol 34:48.

832 52. Lovecká P, Kroneislová G, Novotná Z, Röderová J, Demnerová K. 2023. Plant Growth-Promoting
833 Endophytic Bacteria Isolated from Miscanthus giganteus and Their Antifungal Activity.
834 Microorganisms 11:2710.

835 53. Santana MM, Rosa AP, Zamarreño AM, García-Mina JM, Rai A, Cruz C. 2022. Achromobacter
836 xylosoxidans and Enteromorpha intestinalis Extract Improve Tomato Growth under Salt Stress.
837 Agronomy 12:934.

838 54. Environment Canada, Health Canada. 2015. Final Screening Assessment for Paenibacillus
839 polymyxa ATCC 842; Paenibacillus polymyxa ATCC 55407; Paenibacillus polymyxa 13540-4.
840 En14-230/2015E-PDF. Final Screening Assessment. Government of Canada, Ottawa.

841 55. Yoneda Y, Yamamoto K, Makino A, Tanaka Y, Meng X-Y, Hashimoto J, Shin-ya K, Satoh N, Fujie
842 M, Toyama T, Mori K, Ike M, Morikawa M, Kamagata Y, Tamaki H. 2021. Novel Plant-Associated
843 Acidobacteria Promotes Growth of Common Floating Aquatic Plants, Duckweeds.
844 Microorganisms 9:1133.

845 56. Akhtar SS, Mekureyaw MF, Pandey C, Roitsch T. 2020. Role of Cytokinins for Interactions of
846 Plants With Microbial Pathogens and Pest Insects. Front Plant Sci 10.

847 57. Fu S-F, Wei J-Y, Chen H-W, Liu Y-Y, Lu H-Y, Chou J-Y. 2015. Indole-3-acetic acid: A widespread
848 physiological code in interactions of fungi with other organisms. Plant Signal Behav
849 10:e1048052.

850 58. Koenig RL, Morris RO, Polacco JC. 2002. tRNA Is the Source of Low-Level trans-Zeatin Production
851 in Methylobacterium spp. Journal of Bacteriology 184:1832–1842.

852 59. Wei X, Moreno-Hagelsieb G, Glick BR, Doxey AC. 2023. Comparative analysis of adenylate
853 isopentenyl transferase genes in plant growth-promoting bacteria and plant pathogenic
854 bacteria. Heliyon 9:e13955.

855 60. Frébortová J, Frébort I. 2021. Biochemical and Structural Aspects of Cytokinin Biosynthesis and
856 Degradation in Bacteria. Microorganisms 9:1314.

857 61. Sugawara H, Ueda N, Kojima M, Makita N, Yamaya T, Sakakibara H. 2008. Structural insight into
858 the reaction mechanism and evolution of cytokinin biosynthesis. Proc Natl Acad Sci U S A
859 105:2734–2739.

860 62. Kuroha T, Tokunaga H, Kojima M, Ueda N, Ishida T, Nagawa S, Fukuda H, Sugimoto K, Sakakibara
861 H. 2009. Functional Analyses of LONELY GUY Cytokinin-Activating Enzymes Reveal the
862 Importance of the Direct Activation Pathway in Arabidopsis. Plant Cell 21:3152–3169.

863 63. Seo H, Kim S, Sagong H-Y, Son HF, Jin KS, Kim I-K, Kim K-J. 2016. Structural basis for cytokinin
864 production by LOG from Corynebacterium glutamicum. Sci Rep 6:31390.

865 64. Noor A, Ziaf K, Naveed M, Khan KS, Ghani MA, Ahmad I, Anwar R, Siddiqui MH, Shakeel A, Khan
866 AI. 2023. L-Tryptophan-Dependent Auxin-Producing Plant-Growth-Promoting Bacteria Improve
867 Seed Yield and Quality of Carrot by Altering the Umbel Order. Horticulturae 9:954.

868 65. Kravchenko LV, Azarova TS, Makarova NM, Tikhonovich IA. 2004. The Effect of Tryptophan
869 Present in Plant Root Exudates on the Phytostimulating Activity of Rhizobacteria. Microbiology
870 73:156–158.

871 66. Eze MO, Amuji CF. 2024. Elucidating the significant roles of root exudates in organic pollutant
872 biotransformation within the rhizosphere. Sci Rep 14:2359.

873 67. Fones H, Gurr S. 2015. The impact of Septoria tritici Blotch disease on wheat: An EU perspective.
874 Fungal genetics and biology : FG & B 79:3–7.

875 68. Peng J, Lin T, Wang W, Xin Z, Zhu T, Gu Q, Li D. 2013. Antiviral Alkaloids Produced by the
876 Mangrove-Derived Fungus Cladosporium sp. PJX-41. J Nat Prod 76:1133–1140.

877 69. Mayser P, Wenzel M, Krämer H-J, Kindler BLJ, Spiteller P, Haase G. 2007. Production of indole
878 pigments by Candida glabrata. Med Mycol 45:519–524.

879 70. Mayser P, Wille G, Imkampe A, Thoma W, Arnold N, Monsees T. 1998. Synthesis of
880 fluorochromes and pigments in Malassezia furfur by use of tryptophan as the single nitrogen
881 source. Mycoses 41:265–271.

882 71. Mayser P, Schäfer U, Krämer H-J, Irlinger B, Steglich W. 2002. Pityriacitrin – an ultraviolet-
883 absorbing indole alkaloid from the yeast Malassezia furfur. Arch Dermatol Res 294:131–134.

884 72. Irlinger B, Bartsch A, Krämer H-J, Mayser P, Steglich W. 2005. New Tryptophan Metabolites from
885 Cultures of the Lipophilic Yeast Malassezia furfur. Helvetica Chimica Acta 88:1472–1485.

886 73. Huang D, Zhang Z, Li Y, Liu F, Huang W, Min Y, Wang K, Yang J, Cao C, Gong Y, Ke S. 2022.
887 Carboline derivatives based on natural pityriacitrin as potential antifungal agents.
888 Phytochemistry Letters 48:100–105.

889 74. Machowinski A, Krämer H-J, Hort W, Mayser P. 2006. Pityriacitrin – a potent UV filter produced
890 by Malassezia furfur and its effect on human skin microflora. Mycoses 49:388–392.

891 75. Dai J, Dan W, Schneider U, Wang J. 2018. β-Carboline alkaloid monomers and dimers:
892 Occurrence, structural diversity, and biological activities. Eur J Med Chem 157:622–656.

893 76. Gaitanis G, Magiatis P, Mexia N, Melliou E, Efstratiou MA, Bassukas ID, Velegraki A. 2019.
894 Antifungal activity of selected Malassezia indolic compounds detected in culture. Mycoses
895 62:597–603.

896 77. Wang J, Chen M, Lv Y, Jiang Y, Qiu L. 2016. Edaphobacter dinghuensis sp. nov., an acidobacterium
897 isolated from lower subtropical forest soil. International Journal of Systematic and Evolutionary
898 Microbiology, 66:276–282.

78. Ueda S, Kitani S, Namba T, Arai M, Ikeda H, Nihira T. 2018. Engineered production of kitasetalic acid, a new tetrahydro-β-carboline with the ability to suppress glucose-regulated protein synthesis. J Antibiot 71:854–861.

79. Li X-L, Sun Y, Yin Y, Zhan S, Wang C. 2023. A bacterial-like Pictet–Spenglerase drives the evolution of fungi to produce β-carboline glycosides together with separate genes. Proceedings of the National Academy of Sciences 120:e2303327120.

80. Zuther K, Mayser P, Hettwer U, Wu W, Spiteller P, Kindler BLJ, Karlovsky P, Basse CW, Schirawski J. 2008. The tryptophan aminotransferase Tam1 catalyses the single biosynthetic step for tryptophan-dependent pigment synthesis in Ustilago maydis. Molecular Microbiology 68:152–172.

81. Liew LPP, Fleming JM, Longeon A, Mouray E, Florent I, Bourguet-Kondracki M-L, Copp BR. 2014. Synthesis of 1-indolyl substituted β-carboline natural products and discovery of antimalarial and cytotoxic activities. Tetrahedron 70:4910–4920.

82. Khosravi Babadi Z, Ebrahimipour G, Wink J, Narmani A, Risdian C. 2021. Isolation and identification of Streptomyces sp. Act4Zk, a good producer of Staurosporine and some derivatives. Lett Appl Microbiol 72:206–218.

83. Patz S, Gautam A, Becker M, Ruppel S, Rodríguez-Palenzuela P, Huson D. 2021. PLaBAse: A comprehensive web resource for analyzing the plant growth-promoting potential of plant-associated bacteria. bioRxiv https://doi.org/10.1101/2021.12.13.472471.

84. Eichberg J, Oberpaul M, Hartwig C, Geißler AH, Culmsee C, Vilcinskas A, Böttcher-Friebertshäuser E, Brückner H, Degenkolb T, Hardes K. 2024. Structural characterization and bioactivity profiling of the fungal peptaibiotic tolypin reveal protective effects against influenza viruses. Archiv der Pharmazie 357:e2400384.

85. Brinkmann S, Kurz M, Patras MA, Hartwig C, Marner M, Leis B, Billion A, Kleiner Y, Bauer A, Toti L, Pöverlein C, Hammann PE, Vilcinskas A, Glaeser J, Spohn M, Schäberle TF. 2022. Genomic and Chemical Decryption of the Bacteroidetes Phylum for Its Potential to Biosynthesize Natural Products. Microbiology Spectrum 10:e02479-21.

Acknowledgements

We would like to thank Oliver Schwengers for the assembly and annotation of the genomes. Prof. Dr. Sylvia Schnell and Rita Geißler-Plaum for scientific and technical support of the plant-related experiments. Walter Lanzalonga was supported by the Erasmus+ Programme of the European Union through a student mobility grant. Celine Zumkeller was supported by the dissertation completion grant, offered based on the Gender Equality Concept provided by Justus-Liebig-University Gießen.

Abbreviations

Abbreviations: OSMAC, one-strain–many-compounds; IAA, indole-3-acetic acid; iP, N6-(Δ2-isopentenyl)adenine; PGPT, plant growth–promoting trait; BGC, biosynthetic gene cluster; NRP, nonribosomal peptide; PKS, polyketide synthase; RiPP, ribosomally synthesized and post-translationally modified peptide; MAG, metagenome-assembled genome; UMAP, Uniform Manifold Approximation and Projection; GTDB, Genome Taxonomy Database; antiSMASH, antibiotics & Secondary Metabolite Analysis Shell; iTOL, Interactive Tree Of Life; UHPLC-QTOF-HRMS, ultra-high-

939 performance liquid chromatography–quadrupole time-of-flight high-resolution mass spectrometry;
940 DMSO, dimethyl sulfoxide; MES, 2-(N-morpholino)ethanesulfonic acid; Trp, tryptophan.